Decadal Solar Irradiance Variability in Northern Europe

Kajsa Parding

Dissertation for the degree philosophiae doctor (PhD)
at the University of Bergen

2014

Dissertation date: November 28

Acknowledgements

First and foremost, I would like to thank my supervisors, Jan Asle Olseth, Beate Liepert, and Knut-Frode Dagestad, who's support and encouragement has been essential during the completion of this thesis. Beate has been an endless source of ideas and knowledge, always keeping the big picture in mind, always enthusiastic and curious. Jan Asle has generously shared his extensive knowledge of radiative transfer as well as life, reminding me of the things that are important outside of the PhD bubble.

Since my early days as a clueless master student, Thomas Ackerman and Laura Hinkelman have provided intellectual guidance with impressive patience. During my PhD project, they continued to play an important role in making me into the slightly more knowledgable and savvy soon to be doctor that I am today. My research stay at the University of Washington during the summer of 2012, hosted by Tom and Laura, was (with the exception of this last year) the most productive three months of my PhD period.

I would also like to thank Dag Kvamme and Eldar Gaĉanica at MET Norway for interesting discussions about weather observations, Noel Keenlyside for valuable insights on large scale climate dynamics, Silje Sørland for friendship and thermodynamical expertise, and all the other colleagues at the Geophysical Institute for direct or indirect contributions.

To my family - mom, dad, Sara - I am grateful to have grown up in a home where intellectual curiosity and a sense of adventure was always encouraged. I could not have done this without you. To Inga, my PhD widow, thank you for love and support throughout this challenging experience. To my dear friends Sandhya and Simon, thank you for everything. I look forward to having more time to spend with you.

Abstract

Shortwave (SW) radiation from the Sun is the external energy source on Earth and the fundamental input of energy into the climate system. Variations of the SW radiation and its transfer through the atmosphere can have important consequences for the living conditions on our planet. Previous studies have reported decadal to multi-decadal variations of SW irradiance at the surface of the Earth of magnitudes comparable to those of greenhouse gas forcing. The observed SW trends are known as global dimming (decreasing SW irradiance) and brightening (increasing SW irradiance).

Varying amounts of atmospheric aerosols, humidity, and clouds, and interactions among these factors are likely candidates to explain the observed SW irradiance variability. Understanding the causes of SW irradiance variations is important because it is informative of the past and future of dimming and brightening: SW irradiance variations that are due to anthropogenic activity will continue to depend on the action of humans; SW irradiance variability that is associated with natural climate variability is not within our control, but can be predicted provided that the variations of the climate system are predictable and well understood.

The aim of this thesis is to investigate the observed decadal variability of SW irradiance in northern Europe. The thesis consists of four papers that all concern aspects of atmospheric transfer of SW radiation through the atmosphere including the relationship between clouds and SW irradiance.

Papers I–III consider the role of clouds and large scale atmospheric circulation plays for dimming and brightening in northern Europe. To this end, we develop empirical-statistical models of solar and cloud variables based on the frequency distribution of the Grosswetterlagen (GWL), a classification of European large scale metorological weather patterns. The GWL models are used to evaluate how the frequencies of cyclonic and anti-cyclonic weather patterns influence the SW radiative climate at different sites. In Bergen, Norway, a decrease of SW irradiance and concurrent increase in cloudiness is observed from the 1960s to around 1990. This cloud-induced dimming is traced to an increasing frequency of cyclones and decreasing occurrence of blocking anti-cyclonic systems. The observed large scale circulation changes influence the radiative climate in other parts of northern Europe too, but results presented in paper III indicate that other more local factors such as varying aerosol emissions may have a more dominant influence at some sites (Stockholm, Sodankyla). In the last two decades, a significant increase in SW irradiance is found at many sites in northern Europe in spring (March–April). Our model indicates that this brightening cannot be explained by observed large-scale circulation shifts and we conclude that decreasing aerosol emissions since the late 1980s may be a likely explanation.

Paper IV deals with the absorption of SW radiation by clouds. It connects to the issue of dimming and brightening because the SW absorptivity of clouds

influence the SW signal that satellites retrieve. Hence investigating dimming and brightening via satellite data will depend on the correct estimate of cloud absorption.

This thesis provides an introduction to the factors that influence SW irradiance and their potential contribution to the observed dimming and brightening. We conclude, based on results presented in the four papers, that the relative importance of the large scale atmospheric circulation, clouds, and other factors that influence SW irradiance may vary from site to site and period to period. Therefore, a regional and local scale may be preferable to a global or continental perspective when studying the causes and effects of dimming and brightening.

List of papers

Paper I

Parding, K., Olseth, J. A., Liepert, B. G., and Dagestad, K.-F. (2014). Decadal variability of clouds, solar radiation and temperature at a high-latitude coastal site in Norway. *Submitted to Tellus B.*

Paper II

Parding K., Olseth, J. A., Liepert, B. G., and Dagestad, K.-F. (2014). Influence of atmospheric circulation patterns of local cloud and solar variability in Bergen, Norway. *Submitted to Atmospheric Chemistry and Physics.*

Paper III

Parding, K., Liepert, B. G., Hinkelman, L. M., Ackerman, T. P., Dagestad, K.-F., and Olseth, J. A. (2014). Influence of synoptic weather patterns on solar irradiance variability in northern Europe. *Manuscript to be submitted.*

Paper IV

Parding, K, Hinkelman, L. M., Ackerman, T. P., and McFarlane, S. A. (2011). Shortwave absorptance in a tropical cloudy atmosphere: Reconciling calculations and observations. *Journal of Geophysical Research* 116, D19202

Contents

1 General introduction

Shortwave (SW) radiation from the Sun is the external energy source on Earth and the fundamental input and dominant source of energy of the climate system. Therefore variations of the SW radiation at the top of the atmosphere and its transfer through the atmosphere can have important consequences for the living conditions on our planet. During the past 30 years, studies have reported decadal to multi-decadal variations of SW irradiance at the surface of the Earth of magnitudes comparable to those of greenhouse gas forcing. The observed SW trends are known as global dimming (decreasing SW irradiance) and brightening (increasing SW irradiance) (Stanhill and Cohen, 2001). There are indications that dimming has weakened the hydrological cycle (Liepert and Romanou, 2005). Dimming and brightening can also have a strong effect on plant life, especially at high latitude locations where photosynthesis and therefore the growth rate is limited not only by air temperature but also by light availability. For example, apparent discrepancies between temperature records and tree-ring densities in the Arctic region have been linked to a global dimming of the region (Stine and Huybers, 2014). It has been suggested that the period of reduced warming from the 1950s to 80s at the northern hemisphere is due to a reduction of SW irradiance which partially counteracted global warming (Murphy et al., 2009; Magnus et al., 2011).

The observed decadal SW irradiance variability in Europe is commonly described as a dimming of approximately 3 watts per square meter (Wm^{-2}) per decade from the 1950s to 1980s, followed by a brightening of around 2 Wm^{-2} per decade from the late 1980s to 2000s (Wild, 2012; Stanhill and Cohen, 2001; Liepert, 2002). Similar trends are reported in the US, and in Asia where the dimming continues even after 1980 (Wild et al., 2009). However, the sparsity of solar irradiance measurement sites in land areas outside of Europe and the lack of sites in ocean areas complicates the overall picture. The surface measurement network is far from representative of the entire globe. Satellite measurements of SW irradiance, which have a better coverage of the Earth, have become available only since the 1980s, and can therefore not be used to study the spatial extent of the dimming from the 1950s to 1980s.

Satellite-based measurements of shortwave irradiance indicate that the fluctuations of solar output are at least an order of magnitude smaller than the observed SW irradiance trends at the surface of the Earth (Lean, 2010; Fröhlich, 2011).

It is therefore reasonable to assume that the causes of dimming and brightening are found within the atmosphere. Changes in the amount, distribution and optical properties of aerosols and clouds have been suggested as likely contributions to the varying SW irradiance. The timing and latitudinal variations of observed SW trends coincide with qualitative emission histories of anthropogenic aerosols and are therefore considered a likely cause of the widespread SW trends (Streets et al., 2009). However, there are regions where cloud changes appear to have a dominant influence on observed dimming and brightening (Chiacchio et al., 2010; Liley, 2009).

The attribution of dimming and brightening is complicated by interactions between the SW radiation attenuating factors. For example, aerosols can act as cloud condensation nuclei, thus changing the reflectivity and life time of clouds. Weather conditions also influence the aerosols: precipitation removes aerosol particles from the air, winds determine the transportation of aerosols from emission sources; the atmospheric humidity changes the size and optical properties of hygroscopic aerosols (Tang, 1996).

The literature of dimming and brightening contains a wide variety of methods to separate the effects of aerosols from clouds or anthropogenic from natural SW irradiance variability. The connection between the clouds and SW irradiance can be assessed by comparing cloud and SW irradiance observations (Stjern et al., 2009; Sanchez-Lorenzo et al., 2009), separately assessing SW irradiance of cloud free and cloudy occasions (Liepert, 2002), or inferring a statistical relationship between the cloud cover and SW irradiance to calculate the SW radiative effects of cloud cover anomalies (Norris and Wild, 2007). Methods that require cloud observations are limited by the availability and quality of these data. In paper I of this thesis, cloud and solar observations from Bergen, Norway are investigated with a focus on decadal scale trends and data quality.

An alternative strategy to investigate the cause of dimming and brightening is to assess the causes of cloudiness variations, namely large scale circulation patterns. This is the focus of papers II and III of this thesis. Previous studies have linked the large scale circulation to the SW irradiance via climate indices (diagnostic quantities that measure an important mode of climate variability) or by statistical pattern recognition of the SW irradiance measurements, e. g. principal component analysis (Sanchez-Lorenzo et al., 2009; Chiacchio and Wild, 2010; Chiacchio and Vitolo, 2012). In papers II and III, the large scale circulation contribution to the observed SW variability is calculated based on a daily

classification of European weather patterns, the Grosswetterlagen (GWL). The advantage of using the GWL data set is that rather than describing a specific climate pattern, it provides a more detailed account of the daily synoptic weather situations in Europe, which makes it more versatile and exact.

2 Objectives

The main objective of this thesis is to investigate the decadal variability of SW irradiance in northern Europe. Understanding the causes of SW irradiance variations is an important theme because it is informative of the past and future of dimming and brightening: SW irradiance variations that are due to anthropogenic activity will continue to depend on the action of humans; SW irradiance variability that is associated with natural climate variability is not within our control, but it could be predicted provided that the variations of the climate system are predictable and well understood. SW irradiance variations may have affected the climate in a way that challenge interpretations of climate proxy data (Stine and Huybers, 2014), and while anthropogenic effects would be limited to the last century, natural variations of SW irradiance could have affected the climate also in the pre-industrial era.

The thesis addresses the following questions:

1 Has SW irradiance and cloudiness varied significantly during the 20th century in northern Europe?
2 If so, are the observations compatible with a cloud induced SW irradiance change?
3 If clouds cannot explain the observed SW irradiance variations, are aerosol emissions a plausible explanation of the dimming and/or brightening?
4 What influence does the atmospheric large scale circulation have on the cloudiness and SW irradiance on decadal to multidecadal time scales?

3 Theoretical background

To evaluate all factors that can cause dimming and brightening, both extraterrestrial and atmospheric processes that influence SW radiation should be considered. Some of the SW modifying factors discussed here can be discounted as

probable causes of dimming and brightening on the basis of negligible variations on decadal to multidecadal time scales.

3.1 Solar shortwave radiation

All objects warmer than 0 K (absolute zero) emit radiation. Hotter objects radiate at shorter wavelengths which contain more energy per photon. There is negligible spectral overlap between the radiative energy of the Sun, which has an effective emission temperature of around 5800 K (Iqbal, 1983) and the considerably colder Earth. The separation between the terrestrial and solar spectrum makes it possible to measure the shortwave radiation from the Sun separately from the terrestrial longwave radiation. The spectrum of the solar radiation observed from satellite is shown in Figure 1 (the yellow area in the diagram). The majority of the radiative energy emitted from the Sun is emitted in the visible (400–750 nm) and near infrared range (750–2500 nm), while less solar energy is found in the ultraviolet (<400 nm) (Iqbal, 1983).

The total extraterrestrial SW irradiance on a horizontal surface at the top of the Earth's atmosphere ($\mathrm{SW}{\downarrow}_{\mathrm{TOA}}$) is calculated as follows (Iqbal, 1983).

$$\mathrm{SW}\downarrow_{\mathrm{TOA}} = S_0 (r_0/r)^2 \cos(\theta) \tag{1}$$

where θ is the solar zenith angle; r_0 is the mean sun-earth distance; r is the actual sun-earth distance at a given time, and S_0 is the solar constant, the total SW irradiance at distance r_0 from the Sun.

The solar zenith angle θ varies with the orientation of the Earth's rotational axis with regards to the Sun. For a specific location on Earth, θ is a function of the latitude, the day of the year and the hour of the day. Variations of θ causes the strong seasonal and diurnal cycles of SW irradiance on Earth. As the Earth's orbit is not circular but elliptical, the Sun-Earth distance r also varies throughout the year, shortest in January and farthest in June. The seasonal and diurnal cycles of SW irradiance are considerably stronger than the long term changes, both at the top of the atmosphere and at the surface of the Earth. Therefore SW irradiance observations must be averaged annually or seasonally or otherwise deseasonalised when studying SW irradiance variability on long time scales. The eccentricity, precession and obliquity of the Earth and its orbit also varies in time, but in cycles of 10,000–100,000 years, and θ and r can therefore

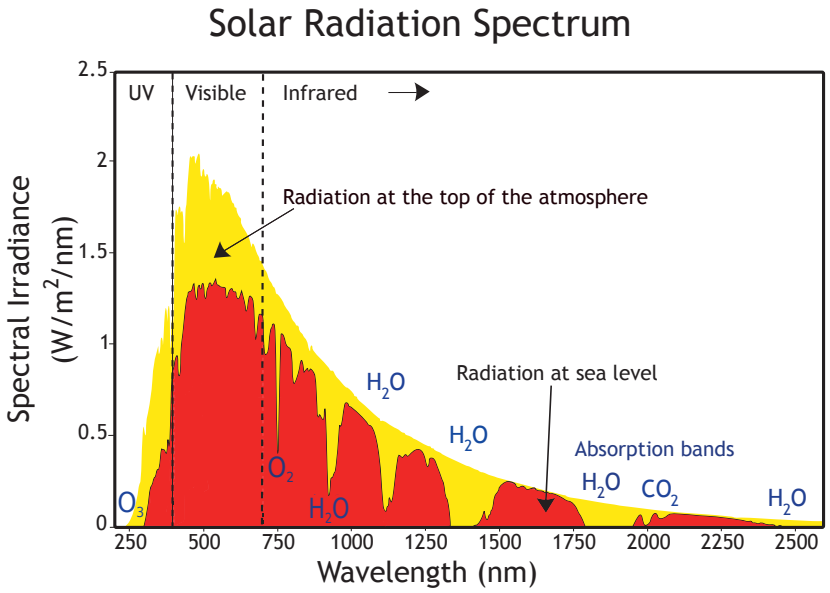

Figure 1: **Spectral attenuation of shortwave (solar) radiation in the atmosphere.** This figure shows the solar radiation spectrum for direct light at the top of the Earth's atmosphere (yellow) and at the surface of the Earth (red). The spectral regions of ultraviolet, visible and infrared light are indicated. As the radiation passes through the cloud-free atmosphere, SW radiation is absorbed by gases with specific absorption bands (O_3, O_2, H_2O, CO_2) which are marked in the figure. In addition, the radiation across the shortwave continuum is scattered by air molecules, some of it reflected back to space. These curves are based on the American Society for Testing and Materials (ASTM) Terrestrial Reference Spectra. (Image prepared by Robert A. Rohde / Global Warming Art.)

be considered stationary on the interannual to centennial time scales which are relevant in the discussion of observed SW variability.

The solar constant S_0 is not really a constant but fluctuates with solar flares and sun spots. Kopp and Lean (2011) reported an approximate S_0 value of 1361 Wm^{-2} in recent measurements. Satellite-based observations of SW irradiance at the top of the atmosphere have been conducted since 1978 and have revealed considerable variations on minute to decade long scales, the most noticeable an 11-year cycle with an amplitude of 0.1 $\%$ (around ± 1 Wm^{-2}) (Fröhlich, 2009; Hathaway, 2010). The latest solar minimum occurred in 2007–2010 and we are currently (2014) in a state of maximum solar radiative output. During the solar cycle, stronger variations occur in the UV wavelength bands. This may may have a considerable effect on the atmospheric circulation as UV radiation has a heating effect in the middle and upper atmosphere where it is absorbed (Ermolli et al., 2013; Haigh et al., 2010). The influence of varying UV radiation is beyond the scope of this thesis. Since the UV radiation constitutes a minor portion of the total radiative energy of the Sun and most is absorbed in the atmosphere (Figure 1), the UV variations have a small direct effect on the total SW irradiance at the surface of the Earth. Reliable estimates of the long-term trends of total solar output are not yet available because of lacking calibration stability of the satellite-based radiometers before 2003 (Lean, 2010). The estimates that exist indicate that the inter-cycle trends are at least one order of magnitude smaller than the SW irradiance variations observed at the surface of the Earth. For example, Fröhlich (2009) estimated a solar output decrease of 0.22 Wm^{-2} between the solar cycle minima in 1986 and 2008, while Willson and Mordvinov (2003) reported an increase of 0.05 $\%$ per decade from 1978 to 2002, which is equivalent of an average S_0 increase of 0.17 Wm^{-2}/decade (Wild, 2009),

3.2 Radiative transfer through the atmosphere

Not all SW radiation that enters the top of the atmosphere reaches the surface of the Earth. The SW radiation is attenuated primarily by interactions with atmospheric molecules, aerosols (particles suspended in the air), and clouds. Figure 1 shows the shortwave radiation spectrum at the top of the atmosphere (yellow area) and at the surface of the Earth (red). The figure demonstrates that the atmospheric attenuation is wavelength dependent and that different

constituents act in different parts of the shortwave spectrum.

The attenuation of SW radiation can be separated into two processes: scattering and absorption. Absorbed SW radiation is re-emitted in all directions as longwave radiation with a wavelength depending on the temperature of the absorbent. Scattering changes the direction of the radiation but not its wavelength.

Particles that are much smaller than the wavelength of the radiation scatter approximately equal in the forward and backward direction. This process, which is called Rayleigh scattering, is highly wavelength dependent, increasing with decreasing wavelength ($\propto \lambda^{-4}$). Scattering by particles comparable to or larger than the wavelength of radiation is calculated with Mie's Theory and does not vary as strongly with wavelength as Rayleigh scattering. Rayleigh scattering is a special case of Mie's theory. Particles that are large compared to the SW radiation (Mie) scatter more strongly in the forward than backward direction.

SW irradiance that arrives on the surface of the Earth in a direct line from the Sun is called direct irradiance. The total scattered SW irradiance that arrives at a horizontal surface from all other directions of the sky dome is referred to as the diffuse irradiance. The total SW irradiance, diffuse+direct, is often referred to as the global irradiance. The word "global" in global dimming refers not to the spatial scale of the phenomenon but to the term global irradiance.

3.2.1 The clean, dry atmosphere

Clean, dry air consists mainly of molecular nitrogen (78 $\%$ N_2), oxygen (21 $\%$ O_2), and smaller amounts of argon (1 $\%$ Ar). The concentration of these constituents varies only on geological time scales and can be considered constant in the context of global dimming and brightening. Other molecules (not water vapour) that occur in smaller concentrations are are called trace gases. Their lifetimes in the atmosphere determine their distribution. Some of the trace gases vary in time and/or space, e. g. carbon dioxide, methane, and ozone.

All air molecules scatter radiation across the shortwave spectrum, more strongly at shorter wavelengths as described by Rayleigh scattering theory. Rayleigh scattering within the atmosphere varies with the air pressure and density, but can be considered stable over long time scales as the concentration of the main molecular constituents of the atmosphere is constant.

Absorption of SW radiation occurs only in limited wavelengths bands which vary depending on the absorbing molecules (Figure 1). For example, ozone (O_3) absorbs most of the incident ultraviolet radiation. Carbon dioxide (CO_2), which is steadily increasing in concentration due to human activities, has absorption bands in the near infrared but the strongest absorption occurs in the longwave spectrum. The varying concentrations of these absorbing gases in the atmosphere have influenced the radiative balance in parts of the spectrum, but the effect on the total SW irradiance is negligible (Barker, 2007; Cutchis, 1974).

3.2.2 Water vapour

Water vapour is a potent absorber of SW radiation with several absorption bands in the near infrared and infrared parts of the solar spectrum (Figure 1). The amount of water vapour in the atmosphere is highly variable, ranging from 0 to 5 $\%$ of the atmospheric concentration by volume depending on the location and time of day (Wallace and Hobbs, 2006). Of the gaseous constituents in the atmosphere, water vapour has the largest potential to modify the total SW irradiance.

Sensitivity studies with radiative transfer models have indicated that it would require large changes of water vapour concentrations to explain the observed SW trends during the 20th century (Wild, 2009). On a global scale, the changes in humidity have not been strong enough to explain the observed dimming and brightening (Wild, 1997). Nevertheless, increasing atmospheric water vapour concentration may have had an important contribution to local or regional dimming, not only through direct absorption of SW radiation but also through its influence on the cloud field (Yang et al., 2012). In a future warming climate, the water vapour concentrations may increase enough to have a strong dimming influence on SW irradiance (Haywood et al., 2011).

3.2.3 Aerosols

Aerosols are dry or liquid particles suspended in the atmosphere. The size, shape, and material composition of aerosols vary greatly, ranging in equivalent radius from 10^{-3} to 10^{2} μm (Iqbal, 1983, Chapter 5). Aerosols have a direct effect on SW irradiance, scattering or absorbing the SW radiation depending on the optical properties of the particles. Smaller particles scatter SW radiation more effectively than larger particles.

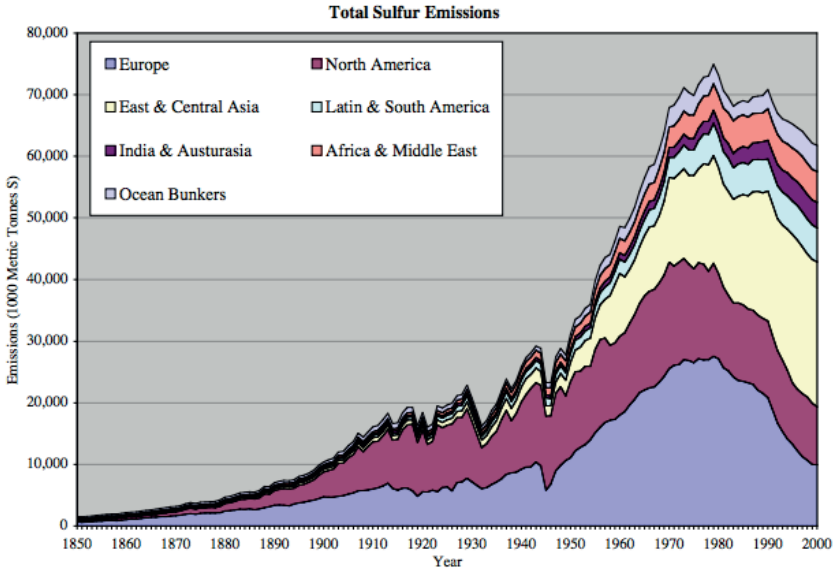

Figure 2: **Global sulfur dioxide emissions by meta-region.** Figure from Smith et al. (2004).

Aerosols can be directly injected into the atmosphere or formed in the atmosphere from gases. These secondary aerosols tend to be smaller (<1 μm) and hence more optically efficient. Gas-to-particle aerosols can form from sulfur, nitrogen, and organic and carbonaceous material. The vast majority of the sulfate and nitrate gas-to-particle aerosols in the northern hemisphere are of anthropogenic origin (Wallace and Hobbs, 2006, Table 5.3).

Dust, pollen, salt from ocean spray, and soot from forest fires are examples of naturally occurring aerosols. Not all natural aerosol sources can be assumed to be stable on decadal to multidecadal time scales. For example, the frequency of forest fires and Sahara dust outbreaks may change considerably over time (Miller et al., 2012; Goudie, 2009). The frequency of such events can be affected by anthropogenic climate change, which muddles the distinction between anthropogenic and natural aerosol changes.

Anthropogenic aerosols come from a variety of human activities, the main sources being road dust, soil dust from agricultural tillage, biomass burning, and emissions from combustion engines and other industrial activities. Sulfuric acid particles occur naturally, from volcanic eruptions, as well as from anthro-

pogenic sources (industrial activities, combustion engines) (Wallace and Hobbs, 2006). Stratospheric sulfur aerosols reflect SW radiation and thus effectively reduce the total SW irradiance.

Volcanic eruptions provide a chance to study the influence of sulfur emissions on SW radiation and the climate system. During recent events, such as the eruption of El Chicón (Mexico) in April-May 1986 and Mount Pinatubo (Philippines) in June 1991, notable reductions of SW irradiance were detected across the globe (Alados-Arboledas et al., 1997). In paper I, we note that the volcanic signals of Mount Pinatubo and El Chicón can be found in Bergen as a temporary increase of the aerosol optical depth.

The anthropogenic sulfur emissions have increased since the 1850s, at an accelerated rate since the 1950s (Figure 2). In recent decades, the emissions have been reduced as a result of stricter regulations on industrial air pollution. The emissions of sulfur oxides (SO_x) in Europe have decreased from approximately 25.8×10^9 kg in 1990 to 4×10^9 kg in 2012 (EEA Technical report, 2014).

3.2.4 Clouds

Clouds scatter and absorb SW radiation. On short time scales – hourly to inter-annual – clouds have a stronger influence on the variations of SW attenuation than any other atmospheric process. The albedo (reflectance) of a cloud and the direction in which the SW irradiance is reflected depends both on the optical properties, ice or water phase, distribution and height of clouds (Kokhanovsky, 2004).

Clouds form when the moist air is supersaturated with respect to water or ice (Wallace and Hobbs, 2006, Chapter 6). Supersaturation occurs when an air parcel is rising to higher altitudes which allows the air to cool adiabatically, by expanding. Sinking air (subsidence) on the other hand warms adiabatically, by compressing, which may evaporate any clouds that are present.

When supersaturation occurs, cloud droplets form upon small particles that are referred to as cloud seeds or cloud condensation nuclei (CCN) (Hudson, 1993). If no CCN are available, very high super-saturation can occur without cloud droplets forming (Katz and Ostermier, 1967). Since CCN are generally present in the atmosphere, super saturation levels above 1–2 $\%$ are rarely found in the atmosphere (Wallace and Hobbs, 2006, Chapter 6). Clouds above the 0°C

altitude level may contain both super-cooled droplets and ice particles. Ice particles form upon the surface of ice nuclei (IN), particles with a molecular structure similar to the hexagonal structure of ice. In the atmosphere, formation of ice particles without IN occur only at high altitudes where the temperature is very low ($< -35^{\circ}$C). In a pristine environment with few aerosols in the atmosphere, cloud droplets tend to be fewer and larger than when there are aerosols available to act as CCN. Assuming all else is the same, an increase of the CCN amount increases the reflectivity of the clouds because the smaller droplets are more reflective. An increasing amount of CCN also hinders cloud droplets from coalescing which inhibits precipitation, thus increasing the lifetime of the clouds (Koren and Feingold, 2011).

There are two basic types of clouds: stratiform and cumuliform. The cumuliform clouds form when air in an unstable atmosphere rises due to heating. The stratiform clouds are formed when a whole layer is forced to rise, often in association with a weather front. With the exception of rare types of ice clouds, clouds are confined to the troposphere, the lowest layer of the atmosphere that contains about 80 $\%$ of the atmospheric mass (Wallace and Hobbs, 2006, Chapter 1). Because the temperature in the troposphere decreases with height, ice and mixed phase clouds occur more frequently at higher altitudes. Low level clouds tend to be more optically thick than their mid and high altitude counterparts.

In the presence of clouds, SW irradiance is attenuated by the clouds as well as by the atmospheric constituents discussed in the previous text. Multiple scattering within or between clouds increases the path length of the SW radiation and therefore increases SW absorption by cloud droplets as well as other absorbing constituents in the atmosphere (Kokhanovsky, 2004). The multiple scattering effect of clouds is discussed in Paper IV.

3.2.5 Interactions among clouds, aerosols, water vapour, and SW irradiance

The atmospheric factors described above are not fully independent. Aerosol particles can influence SW radiation indirectly by acting as cloud condensation nuclei, thus modifying the albedo (reflectivity) and life time of clouds. In heavily polluted regions, absorbing aerosols can also stabilise the atmosphere by heating which has a suppressing effect on cloud formation, known as the semi-direct aerosol effect.

The atmospheric conditions influence aerosols. The wind direction influences the transportation of aerosols from the source of emissions. Precipitation and atmospheric turbulence influence the deposition of aerosols, which affects both total amount and the size distribution of the particles. Atmospheric humidity influences the size and therefore the optical properties of hygroscopic aerosols.

Changes of SW irradiance can also influence cloud formation and atmospheric circulation. By affecting evaporation, changes in SW irradiance may also have some influence on the ocean salinity which can indirectly lead to changes in the sea surface temperatures and atmosphere-ocean heat exchange (Durack et al., 2012; Pierce et al., 2012). All of this may feedback to the SW irradiance via the distribution of clouds, humidity, and wind.

3.3 Large scale circulation patterns

Large scale or synoptic weather patterns refers to meteorological structures of horizontal scales of the order of 1000 km. At mid and high-latitudes, the most commonly occurring synoptic weather patterns are low and high-pressure systems. The winds in the Earth's atmosphere flow closely parallel to the isobars (lines of constant pressure), in a cyclonic flow around the low pressure centres (counter clockwise on the northern hemisphere) and in an anticyclonic flow around the high pressure centres (counter clockwise on the northern hemisphere). The low and high pressure systems at mid-latitudes migrate eastward along paths steered by planetary waves, also known as Rossby waves. The general atmospheric circulation is driven by differential heating and modified by the rotation of the Earth. For a thorough introduction to the atmospheric dynamics and synoptic meteorology, see, e. g. of Wallace and Hobbs (2006) (chapters 7 and 8) or Holton (2004).

The large scale circulation influences the local SW irradiance at a site primarily via the distribution of clouds and humidity. Cyclonic weather patterns are associated with clouds and precipitation. The cloud formation is a result of rising air which cools adiabatically. Much of the weather associated with cyclones tends to be concentrated along frontal zones which mark sharp shifts in temperature and winds. Frontal zones form when a warmer and a cooler air mass meet and the warm air which is less dense rises above the cold air. Anti-cyclonic weather patterns are associated with cloud-free conditions as a result of subsidence.

The circulation patterns may also affect the SW irradiance via the influence of wind direction and precipitation on aerosol transportation and deposition. In addition, the atmospheric circulation may be influenced by human-induced climate change (Bengtsson et al., 2006; Wu et al., 2010). Hence, even when the atmospheric circulation-driven SW irradiance variability is successfully separated from the SW variability due to other factors, the natural SW irradiance variability may not be fully separated from anthropogenic influence.

4 Observational data

4.1 SW irradiance measurements

4.1.1 Instrumentation

Global irradiance (total SW irradiance on a horizontal surface on Earth) is measured by the pyranometer, a radiometric instrument with a hemispheric view of the sky dome. A pyranometer consists of a flat sensor that absorbs the incoming SW radiation and converts it to a signal that can be related to the total absorbed energy. The sensor is covered by a glass dome that limits the radiation to wavelengths within the shortwave range (≈280–2800 nm) and keeps it dry and clean (Goswami et al., 2000, Chapter 2.7.1). Radiometers tend to drift gradually as the detector surface becomes less efficient. The instruments must therefore be calibrated regularly (Reda et al., 2003) and eventually replaced.

The diffuse irradiance is measured by a pyranometer with a shadow band or disc mounted on it that shadows the direct sunlight. The shadow band or disc follows the track of the sun as it moves across the sky. The direct irradiance is measured by a pyrheliometer, a radiometer with a detector shielded to restrict the view to about 5° of the sky. The pyrheliometer must always be pointed toward the sun and requires a sun tracker.

4.1.2 Data availability

Observational studies of global dimming and brightening are limited by data availability. Surface-based observations of SW irradiance have been conducted at at few sites in Europe since the 1920s and more widely since the 1950s. During the International Geophysical Year (IGY) in 1957, many observational sites were

established, but still the southern hemisphere and regions outside of Europe are underrepresented, as seen in Figure 3 which shows the observational stations of the Global Energy Balance Archive (GEBA, Gilgen and Ohmura (1999)).

The GEBA data base offers monthly averaged quality controlled SW irradiance measurements which have been used in many studies of dimming and brightening, e. g. Stanhill and Cohen (2001), Gilgen et al. (2009), and Chiacchio and Wild (2010). Many of the same historical SW irradiance records are also available as daily averaged time series from the World Radiation Data Center (WRDC) of the Main Geophysical Observatory, St. Petersburg, available for the period 1964–1993 via the joint website of WRDC and the National Renewable Energy Laboratory (http://wrdc-mgo.nrel.gov/) or for 1964 to the present day directly via the WRDC website (http://wrdc.mgo.rssi.ru/). The relative uncertainty of the historical measurements of the GEBA/WRDC data base has been estimated to approximately 5 % for the monthly mean and 2 % of the annual mean, although the measurement quality may vary between individual sites (Gilgen et al., 1998). Data from the GEBA and WRDC data sets are used in paper III.

Since the 1990s, measurement networks offering SW irradiance and auxiliary observations of improved accuracy and high sampling frequency (minute) have been established, e. g. the Atmospheric Radiation Measurement (ARM) Program (Stokes and Schwartz, 1994), and the Baseline Surface Radiation Network (BSRN) (Ohmura et al., 1998) which include observational sites at all continents of the world. In paper IV, SW irradiance observations from an ARM site at the island Manus in the tropical western Pacific are analysed.

In papers I and II, hourly SW irradiance observations from the Geophysical Institute in Bergen from 1965–2013 are used. The data are examined for quality and consistency in paper I. Long SW irradiance time series of hourly or higher resolution are not widely available via an international online archive but can often be obtained by personal communication with the institutes that conduct and collect the measurements.

4.1.3 Satellite-based SW irradiance measurements

Satellite-based measurements have a superior spatial coverage compared to surface-based observations, especially over ocean surfaces. The SW irradiance

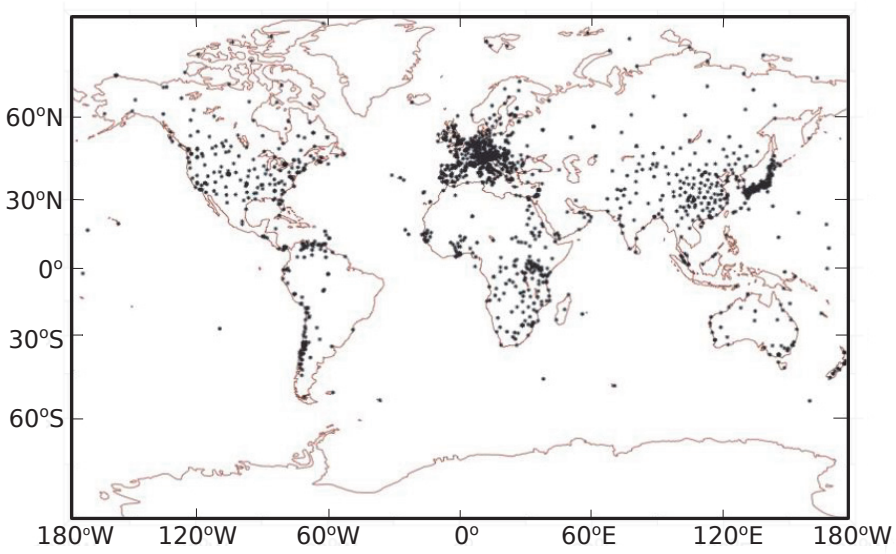

Figure 3: Measurement stations of the Global Energy Balance Archive (GEBA) for which at least one year of data are available that have not been flagged as erroneous by the GEBA quality controls.

at the surface of the Earth is not directly observable from satellite, but can be estimate based on the reflected SW radiance measured by space borne instruments viewing the Earth (Pinker et al., 1995). The first quantitative estimates of surface SW irradiance from satellite were made in the 1970s by (Hanson, 1971) and Ellis and Vonder Haar (1977). Methods of obtaining surface SW irradiance values based on satellite measurements range from simple empirical statistical relationships to more complex radiative transfer models. The conversion of the satellite-based measurements introduces uncertainties and requires assumptions about the absorbing and scattering constituents of the atmosphere. The problems associated with satellite observations with regards to SW absorption in the atmosphere are discussed in paper IV.

4.1.4 Sunshine duration measurements

The sunshine duration is the period of bright unobscured sunshine in a day. It is commonly measured by the Campbell-Stokes sunshine recorder, an instrument consisting of a glass sphere that focuses the incoming solar radiation on to a paper strip (Stanhill, 2003). The beam burns the paper strip when the direct shortwave irradiance exceeds a threshold (the standard is 120 Wm^{-2} but it may vary considerably between instruments). The first sunshine duration measurements by burning glass method were made in 1853 by J F Campbell (Stanhill, 2003). Sunshine duration measurements have been used in previous studies of global dimming and brightening (Sanchez-Lorenzo et al., 2008; Wang, 2014). Compared to the observed SW irradiance, the binary sunshine duration is not sensitive to changes in the optical properties of clouds because it is a threshold measurement. The sunshine duration measurements have the advantage of being remarkably stable over time and the instruments do not have to be regularly replaced, though the paper strips have to be replaced daily. Papers I and II include trend analyses of sunshine duration measurements from Bergen.

4.2 Cloud observations

Clouds have long been measured by visual inspection. Observations by cloud lidar are not as widely available and only for the last few decades. Observations made by humans are limited to the properties of the cloud field that can be estimated by visual evaluation. The standard variables assessed are the cloud

amount, cloud base height, and the cloud amount and type at the low (< 1.5 km), middle ($1.5 - 6$ km) and high (> 6 km) cloud levels (World Meteorological Organization, 2008). The subjective nature of visual cloud observations introduces a large uncertainty. Artificial shifts may occur as individual observers or observational routines change.

Visual cloud observations are available from the Extended Edited Cloud Report Archive (EECRA) for worldwide land sites from 1971 to 2009, and from ship observations for 1951 to 2008 (Hahn and Warren, 1999). Longer cloud records may be available from other sources. For example, the cloud observations used in papers I and II are obtained from the climate data base of the Norwegian Meteorological Institute, eklima (http://www.eklima.no).

4.3 Sea level pressure data

The NCEP-DOE Reanalysis 2 is a reanalysis data set provided by the NOAA Earth System Research Laboratory in Boulder, Colorado (Kanamitsu et al., 2002). The gridded sea level pressure (SLP) data of the NCEP-DOE Reanalysis 2 is used in papers II and III and in Chapter 6 of this thesis to visualise the spatial pressure fields associated with large scale weather patterns.

5 Trend analysis of SW irradiance time series

5.1 Quantifying trends

Global dimming and brightening is often quantified by fitting a linear regression line to individual site records of SW irradiance over a particular time period. This is a convenient method for comparing changes in multiple locations in a region.

Linear trends can be estimated by the least squares method as the slope b of a line, $\hat{y} = a + bt$. Given n time-value pairs (t_i, y_i), the slope is calculated as follows.

$$b = \frac{\sum_{i=1}^{n}(y_i - \bar{y})(t_i - \bar{t})}{\sum_{i=1}^{n}(t_i - \bar{t})^2} \tag{2}$$

$$\text{where} \quad \bar{y} = \sum_{i=1}^{n} y_i \quad \text{and} \quad \bar{t} = \sum_{i=1}^{n} t_i$$

Often, the trend is fitted for the full period of available data or for two separate periods with a change point selected on the basis of some criterion, e. g. the maximum or minimum points of the time series, a second or third order polynomial fit (Wild, 2012). In paper III, SW irradiance trends for ten northern European sites are estimated. The periods of dimming and brightening are then decided based on the minima and maxima of the locally weighted regression smoothed (lowess) curves of the regional average.

In general, linear trends are not always the best description of the way a change takes place. Non-linear and sudden shifts may occur. Calculating the change in the mean value of a variable from one period to another can be an alternative to estimating a linear trend (see, e. g. Liepert (2002)). This approach is taken in Paper I when estimating the seasonal change of solar and cloud observations.

5.2 Statistical significance of trends

The statistical significance of a trend is a measure of the confidence with which the null hypothesis of *no trend* can be rejected. Results of the statistical significance tests are often expressed as the probability, p, of obtaining the estimated trend value from a time series that has no underlying trend. The null hypothesis can then be rejected with a confidence level of $(1 - p) \times 100\%$. Another alternative is to estimate the confidence intervals of the trend values.

The 95 $\%$-level is commonly used as a limit to decide what is statistically significant and what is not. This is a rather arbitrary choice and will in approximately 5 of 100 cases pass a non-significant trend off as a significant trend. Nevertheless, in papers I, II and III, the 95$\%$-significance level is used as a limit to identify significant trends. When possible, the estimated p-values are also reported.

The failure to reject the null hypothesis is not unequivocal proof that no change is happening. It only means that the null hypothesis of *no trend* cannot be rejected. Based on a significance test, we cannot exclude the possibility of an underlying trend that is small compared to the interannual variability. On the other hand, if a trend is so small that it cannot be statistically detected, it may not be of great physical importance either. It is important to keep in mind that not all statistically significant trends are necessarily physically relevant. The magnitude of the trend must also be considered when evaluating if a trend represents an important change.

5.2.1 The student's t-test

Student's t-test is a common test of statistical significance that can be applied to trend estimates. The t-test statistic is the ratio of the magnitude of the trend and the standard deviation of the trend estimate. The t-test assumes that the data follow a normal distribution. Variations of the t-test can also be applied to other statistical measures, e. g. the correlation or the difference between the mean values of two distributions.

5.2.2 The Mann-Kendall test

In papers I, II and III, the statistical significance of the linear trends are estimated by the Mann-Kendall test, a nonparametric test of monotonic change in a time series (Kendall, 1970). The test is conducted using a package called *Kendall* for the programming language and software R. For normally-distributed time series, the t-test has a slightly higher power to detect trends than the Mann-Kendall test, but the difference is small. However, for non-normally distributed data, the power of the Mann-Kendall test is much higher than the power of the Student's t-test (Yue and Pilon, 2004).

The Mann-Kendall test statistic, S, is calculated as follows.

$$S = \sum_{i=1}^{n-1} \sum_{j=i+1}^{n} \operatorname{sign}(y_i + y_j), \tag{3}$$

$$\text{where} \quad \operatorname{sign}(y_i + y_j) = \begin{cases} 1, & \text{if } y_i + y_j > 0; \\ 1, & \text{if } y_i + y_j = 0; \\ -1, & \text{if } y_i + y_j < 0; \end{cases}$$

where y_i and y_j are sequential values of the time series y of length n.

A normalised test statistic Z is then calculated.

$$Z = \begin{cases} (S-1)/\sqrt{\operatorname{var}(S)}, & \text{if } S > 0; \\ 0, & \text{if } S = 0; \\ (S+1)/\sqrt{\operatorname{var}(S)}, & \text{if } S < 0; \end{cases} \tag{4}$$

where var(S) is the Mann-Kendall test variance which is a measure of how much the individual values of S vary around the mean value. The Mann-Kendall test

variance is estimated as

$$\mathrm{var}(S) = \frac{1}{18}\left[n(n-1)(2n+5)\right] \quad (5)$$

where n is the total number of data points.

The probability p associated with the normalised test statistic Z, is obtained by assuming that Z comes from a normal distribution of width 1 and mean 0. For a two-sided test (assuming both positive and negative trends are possible), the p-value is estimated as $p = 2(1 - \mathrm{cdf}(|Z[]))$, where cdf is the cumulative distribution function for the normal distribution. Values of p lower than 0.05 indicate that the estimated trend is statistically significant at the 95 $\%$-level.

The Mann-Kendall test as described above assumes that there is no serial autocorrelation of the data. Positive autocorrelation increases the probability of detecting a trend where there is none and negative autocorrelation has the opposite effect. The variance, var(S), can be modified to compensate for autocorrelation of a time series (Blain, 2013; Hamed, 2009; Hamed and Ramachandra Rao, 1998). However, the variance modifications have the side effect of reducing the power of the Mann-Kendall test when the data are truly independent (Hamed and Ramachandra Rao, 1998). The annually and seasonally averaged solar and cloud observations studied in papers I, II and III are not strongly autocorrelated and applying the variance modification was therefore deemed unnecessary.

5.3 Visualising trends for multiple time periods and change points

Estimating the trend for a single period cannot capture the full complexity of decadal SW irradiance variability. An alternative approach is to calculate trends for a multitude of periods to avoid the more or less arbitrary choice of change points. The results can be presented visually as in Figure 4, which shows the trend analysis of the annual mean SW irradiance observed in Toravere, Estonia from 1955 to 2009. Based on visual inspection of the time series in Figure 4a, there is a decrease of SW irradiance, i. e. a dimming, from the 1960s to the mid 1980s, followed by a partial recovery, a brightening.

Figure 4b shows the magnitude of linear trends for sliding 30 year periods. In this plot, statistically significant trends are marked with large circular markers

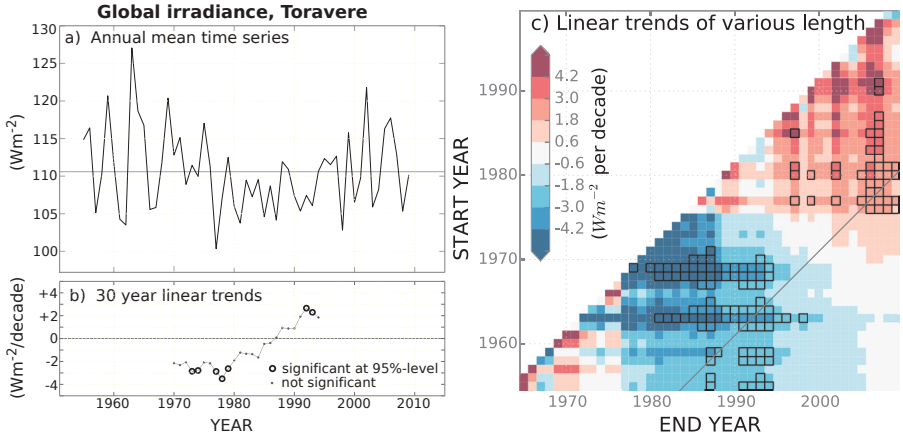

Figure 4: Trend analysis of the observed global irradiance observed in Toravere, Estonia. The three panels show a) the annual mean time series for 1955–2009, b) sliding 30 year long linear trends, and c) linear trends for periods of various lengths. In panel b, the x-axis represents the centre year of each period for which a linear trend has been estimated (period = [centre - 15 years, centre + 14 years]). Periods with trends that are significant at the 95 %-level are marked by large circles in the sliding trend diagram (b) and with black edges in the multiple trend diagram (c).

(95 $\%$ significance level, Mann-Kendall test). The trend estimates confirm the visual impression of Figure 4a, that there is a dimming followed by a brightening in Toravere. For example, from 1958 to 1987 there is negative SW irradiance trend of approximately -3 Wm^{-2}, and from 1977 to 2006, a positive trends of almost the same magnitude. Both of these trends are statistically significant at the 95 $\%$-level.

Figure 4c shows the estimated trends of all periods that are longer than 10 years. The x- and y-axes represent the end and start year of each period and the magnitude of the linear trend is displayed as a colour, red denoting positive trends and blue denoting negative trends. Periods for which the estimated trend is statistical significant at the 95 $\%$-level are marked with black edges. The 30 year long periods displayed in panel b are marked as a black diagonal line.

The trend diagram in Figure 4c illustrates that the estimated magnitude and statistical significance of a trend is highly dependent on the exact period that is considered. The length of the considered period influences the power of the statistical test to distinguish a trend from background noise (Hinkelman et al., 2009). The smaller the sample size, the stronger the trend signal has to be to be statistically significantly identified.

In papers I and II, a sliding trend analysis as demonstrated in Figure 4b is used to quantify and visualise the trends of SW irradiance and clouds in Bergen. The method displayed in Figure 4c gives a more complete picture of the changes that occur but is impractical when comparing the trends of several time series.

5.4 Is there a dimming and brightening in Europe?

The monthly SW irradiance time series of the GEBA data base have been used in many studies of dimming and brightening (Ohmura, 2009; Gilgen et al., 2009). Here, SW irradiance observations from GEBA sites in Europe are analysed to assess the spatial extent and regional characteristics of dimming and brightening in Europe. Only measurement sites with less than 24 missing monthly observations during 1965–2004 are included. The strict data availability requirements leave only the 33 measurement sites depicted in Figure 5. The sites are divided into two groups, north and south of 55°N. The ten sites north of 55°N are analysed further in paper III. The selected subset of observational stations does not cover any parts of France, the Iberian Peninsula or Italy and includes only few sites

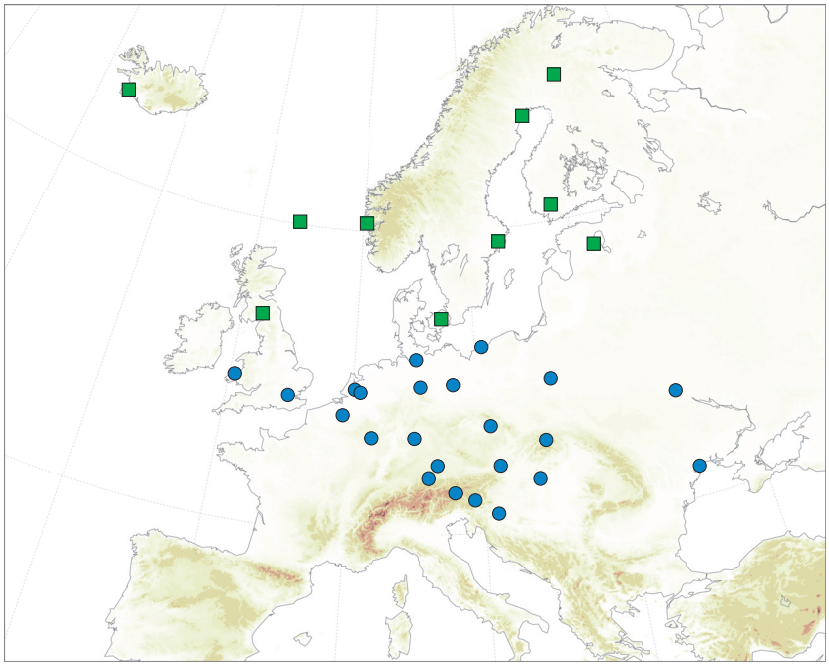

Figure 5: Map of Europe showing the SW irradiance measurement sites that are analysed in Figures 6 (green squares) and 7 (blue circles). The SW irradiance data are available via the Global Energy Balance Archive (GEBA). The sites have been selected on the basis that they have few (<24 months) missing data between 1965 and 2004.

in eastern Europe. No steps are taken to ensure spatial representativity and the results of the following trend analysis should therefore be interpreted with some caution.

Figures 6 and 7 show multiple trend diagrams which summarise the decadal variability of the SW irradiance observed at the individual sites within the two European regions. The plots are similar to the trend diagram in Figure 4c, with the y- and x-axes showing the start and end year of each period. Here, the colour scale represents the number of sites that undergo a strong SW irradiance trend during each period. The number of sites that experience a dimming and brightening are plotted separately in the left and right hand side panels, respectively. In the upper panels, the dimming and brightening are defined as linear trends stronger than 2 Wm^{-2} per decade. The lower panels count only

sites with trends that are statistically significant at the 95 $\%$-level, estimated by the Mann-Kendall test. Similar multiple trend diagrams are commonly used in hydrological studies, e. g. McCabe (2002) and Schmocker-Fackel and Naef (2010).

The majority of the sites in northern Europe experience negative SW irradiance trends ($< -2Wm^{-2}$/decade) from the late 1960s to the early 1990s (Figure 6). However, the estimated trends are statistically significant at less than half of the sites. Positive trends are detected from the late 1980s to the 2000s at a majority of the sites, but the brightening trends are significant only at a few of the sites.

For the 23 sites in Europe south of 55°N, the multiple trend analysis reveals an earlier shift from dimming to brightening compared to northern Europe (Figures7). Positive SW irradiance trends occur at more than half of the sites from the late 1970s to the 2000s, significant at more than 10 of the 23 sites. A dimming period is seen from the 1960s to the 1980s, but the negative SW irradiance trends are statistically significant at only a few sites.

Figures 6 and 7 demonstrate that in many cases, even strong linear slopes ($>$2 Wm^{-2}/decade) are not statistically significant. Strictly speaking, few of the time series have a statistically detectable dimming and brightening. Nevertheless, the similarities within the regions can be interpreted as an indication of the presence of large scale processes influencing the SW irradiance on decadal time scales.

To isolate the processes that may be causing the wide spread observed SW irradiance variations, regionally averaged time series can be calculated. Depending on the spatial extent of the region, the averaging may reduce or emphasise the influence of large scale weather patterns on SW irradiance. Figure 8 shows the regionally averaged annual mean SW irradiance for the regions discussed above. The regional average of the 23 sites south of 55°N shows no significant dimming but a considerable and statistically significant brightening in recent decades. In contrast, the northern European regional average shows a significant dimming from the 1970s to around 1990 but not much sign of a brightening. The regional trend analysis in paper III shows that there is a significant brightening in northern Europe in spring, but obviously it is not as prominent when considering the annual mean SW irradiance.

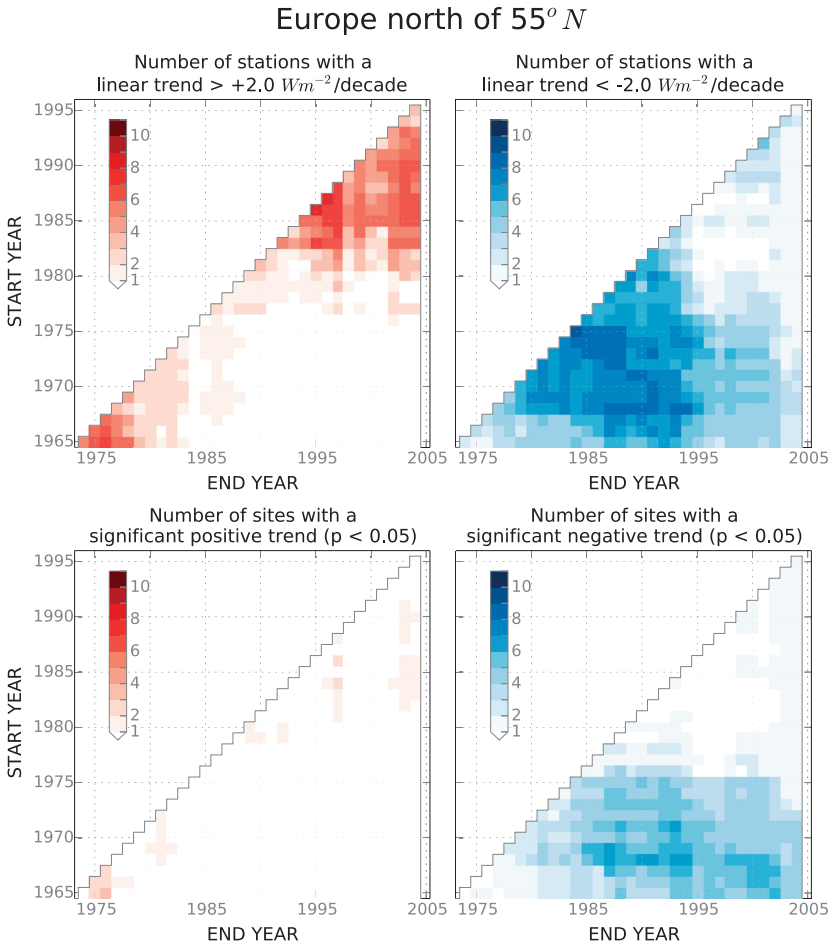

Figure 6: Trend analysis of the observed SW irradiance for a group of 10 measurement sites in Europe north of 55°N (see map in Figure 5). The y- and x-axes of the diagrams indicate the start and end of each analysed period and the colour scale represents the number of sites that have a positive (upper left panel) and negative (upper right panel) global irradiance trend stronger than 2 Wm^{-2}/decade. The lower panels show the same analysis but with the requirement that the trends must be statistically significant at the 95 %-level ($p < 0.05$, Mann-Kendall test).

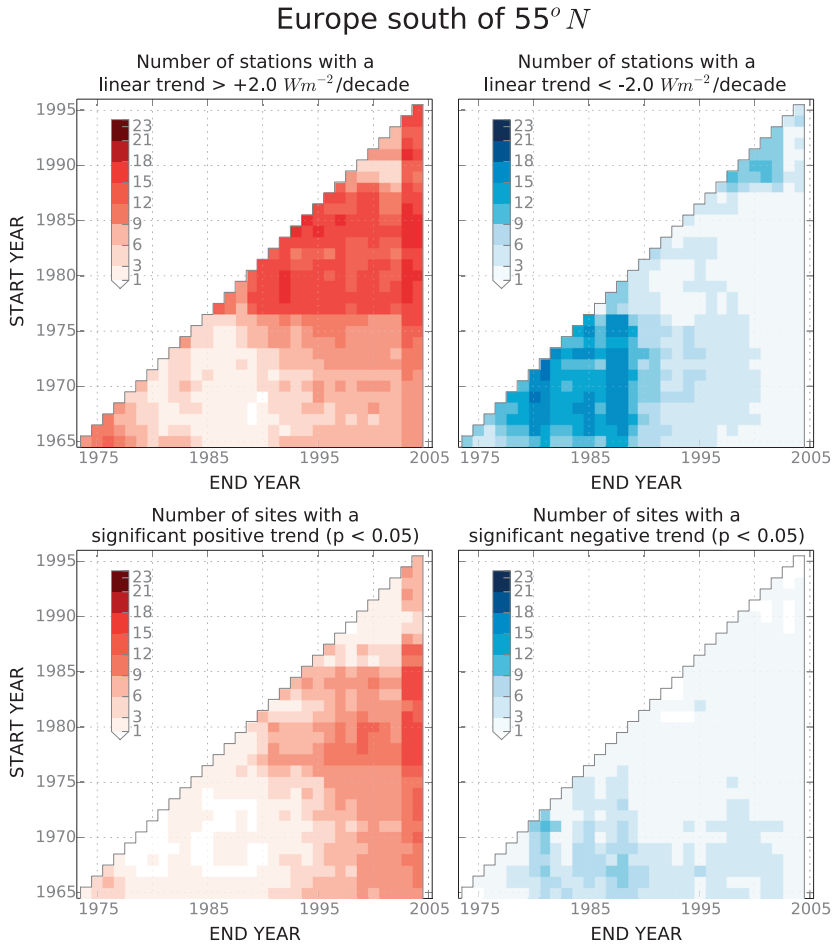

Figure 7: Like Figure 6 but for a group of 23 sites in Europe south of 55°N (see map in Figure 5).

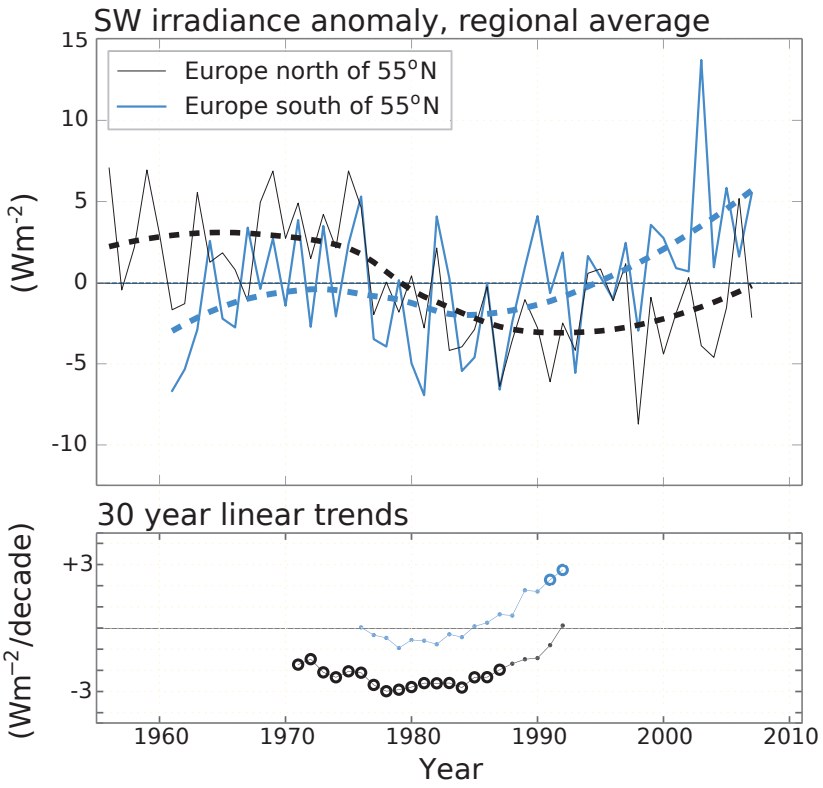

Figure 8: Regionally averaged time series of SW irradiance for the two groups of measurement sites north and south of 55°N shown in map Figure 5. The time series and trends are plotted as in Figure 4a and b. The upper panel includes, in addition to the annual mean SW irradiance (solid lines), also a lowess smoothed curve with a 40 year smoothing window (dashed lines).

6 Grosswetterlagen - large scale weather patterns of central Europe

In papers II and III, the connection between large scale and local weather conditions is investigated. As a measure of the large scale circulation patterns, we use a subjective weather pattern classification, the Grosswetterlagen (GWL). The GWL data set offers a daily record of the large scale weather patterns over Europe and the north Atlantic region since 1881.

The GWL data set represents 29 weather patterns whose definition is based on the atmospheric flow over central Europe. This weather pattern classification was first developed by Baur et al. (1944) in the 1940s, revised by Hess and Brezkowsky in 1950-1951, and maintained by the German weather service (Werner and Gerstengarbe, 2010).

The GWL are characterised by the position of cyclonic and anti-cyclonic weather systems and the direction of the surface flow over central Europe. The classification is based on visual inspection of Sea Level Pressure (SLP) and 500 hPa geopotential height observations of the North Atlantic and Europe.

Each day since 1881 has been prescribed exactly one GWL. The weather pattern must persist unchanged for a minimum of 3 days, or it is prescribed as unknown, which is rare (unclassified days occur in less than $< 1\%$ of all days 1881–2014). That is not to say that the synoptic weather situation does not change on time scales shorter than 3 days, but that the GWL describe large scale atmospheric circulation structures that change only slowly.

To illustrate how the GWL relate to the synoptic weather patterns over Europe, Figures 9 and 10 show daily averaged sea level pressure (SLP) maps for two separate periods in July 1990.

Figure 9 shows the progression of cyclonic systems travelling eastward over Scandinavia from July 1 to July 9, 1990. All days during this period have been identified as GWL 2, also known as WZ or "Westlage Zyklonen" (westerly cyclonic) which refers to the westerly flow and cyclonic weather pattern over central Europe. The atmospheric circulation pattern is obviously not static during the nine days, but the large scale structure remains the same.

Figure 10 shows a developing blocking event later in the same month, July 22–30, 1990. There is a gradual progression of the anticyclonic systems, the high

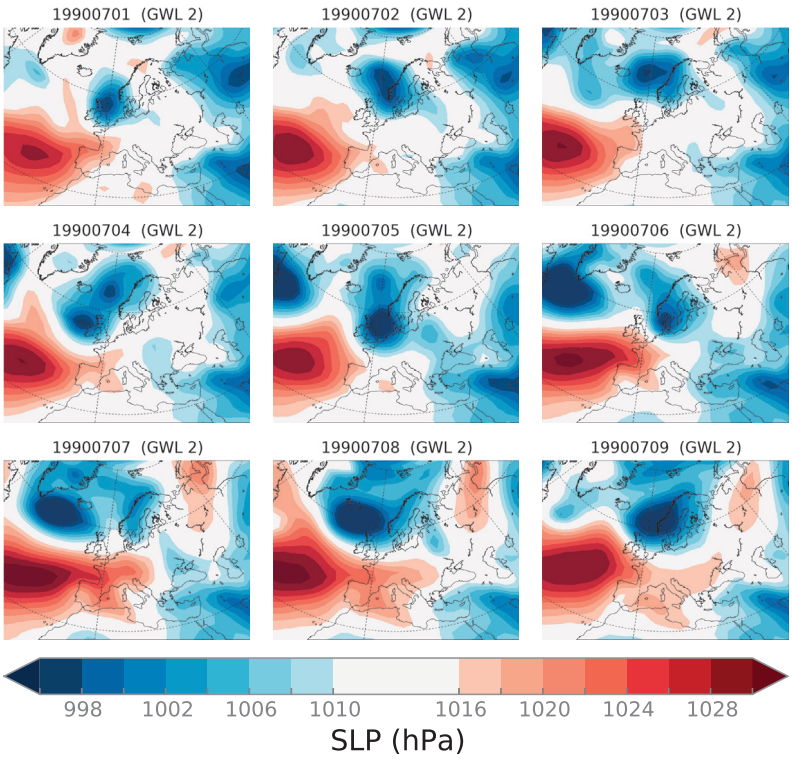

Figure 9: Daily average sea level pressure maps for the period July 1–9, 1990, during which all days were identified as the weather pattern GWL 2, characterised by a westerly cyclonic flow over central Europe.

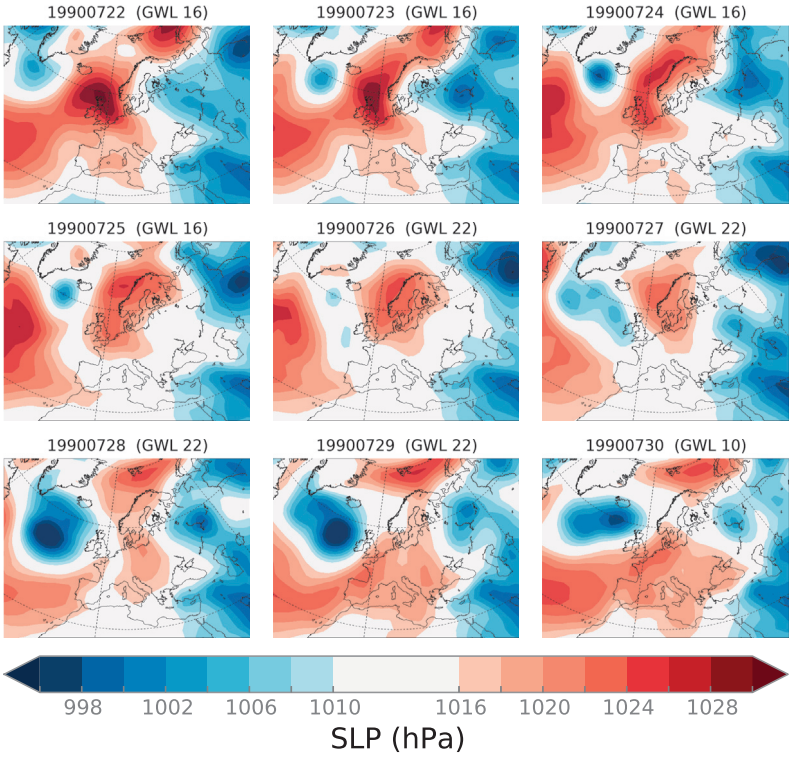

Figure 10: Daily average sea level pressure maps for the period July 22–30, 1990, a developing blocking situation described in the GWL data set as a progression from GWL 16 (high over British Isles) to GWL 22 (high over the Norwegian Sea and Fenno-Scandianavia) to GWL 10 (high pressure ridge over central Europe).

pressure system shifting its centre from the British Isles to Scandinavia and finally to a situation with high SLP over central and southern Europe and another high over the Barents Sea. In the GWL data set the development is represented as a discrete succession of weather patterns, each lasting a minimum of three days: First GWL 16 (HB = Hoch Britisch Inseln = high over British Isles) from July 22 to 25, then GWL 22 (HNFA = Hoch Nordmeer-Fennoskandien, Antizyklonal = high over the Northern Sea and Fenno-Scandinavia (Scandinavia, Finland and Karelia) and anticyclonic flow over central Europe) from July 26 to 29, and finally a shift to GWL 10 (BM = Hochdruckbrücke (rücken) Mitteleuropa = high-pressure ridge over central Europe) on July 30.

Figure 11 shows the average SLP patterns of all days classified as GWL 2, 10, 16 and 22, the weather patterns that occurred in the examples discussed above. The average SLP maps represent the large scale structures associated with the GWL. The figures demonstrate that the daily features of the synoptic weather patterns (Figures 9 and 10) are smaller and change faster than the large scale structures that the GWL describe.

The influence of cyclonic and anti-cyclonic systems on the distribution of clouds is evident in Figure 12, which shows the correlation between the surface observed cloud cover and the frequency of the four previously discussed weather patterns, GWL 2, 10, 16 and 22. Significant positive correlations between the cloud cover and the frequency of GWL 2 are found in the regions where this weather pattern is associated with low SLP (northern and western Europe, see Figure 11). For GWL 10, 16, and 22, significant negative correlations between cloud cover and weather pattern frequency are found in the high SLP regions. In summary, the GWL weather patterns are associated with reduced (increased) cloudiness in the regions where the high (low) pressure systems tend to be centred.

6.1 Empirical GWL models

In papers II and III, empirical models of local solar and cloud observations are constructed based on the frequency of occurrence of the 29 GWL weather patterns. The empirical models are used to investigate the influence of large-scale weather patterns on local SW irradiance variability. The direct and indirect effects of changing aerosol emissions are also estimated as the difference between the observed and modelled normalised SW irradiance.

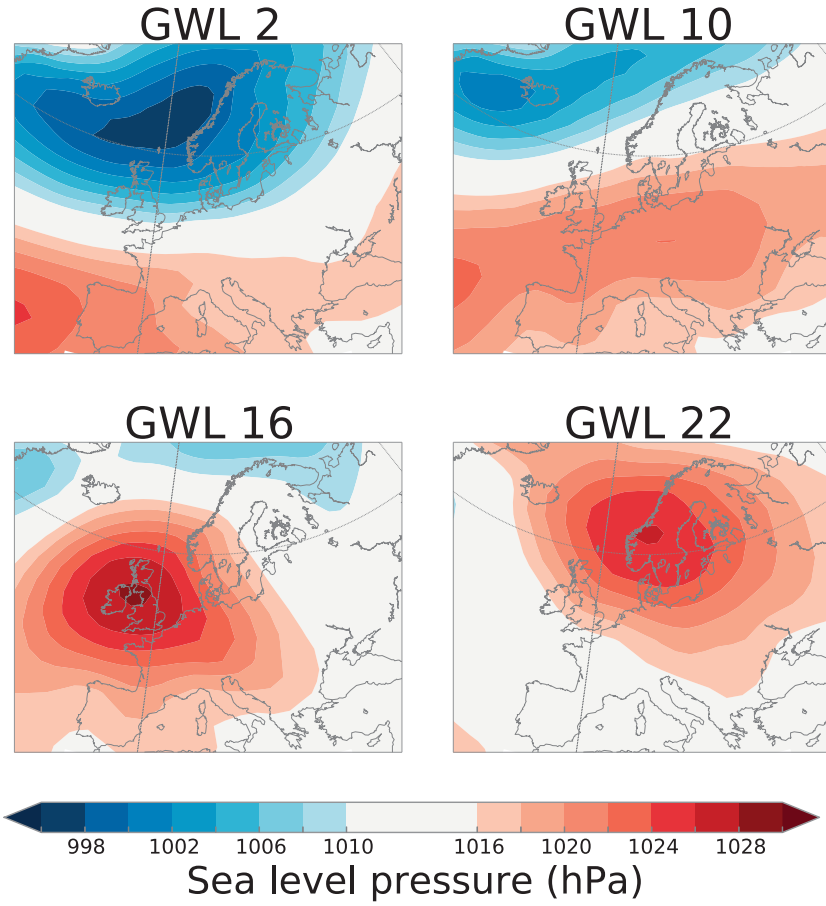

Figure 11: Maps of the average sea level pressure (SLP) patterns over Europe and the north Atlantic associated with four of the 29 Grosswetterlagen weather classes. The maps are calculated from daily gridded SLP data from the period 1979–2009 (the extent of the SLP data set). For example, the SLP map of GWL 1 is calculated as the average SLP in each grid cell during all days classified as GWL 1.

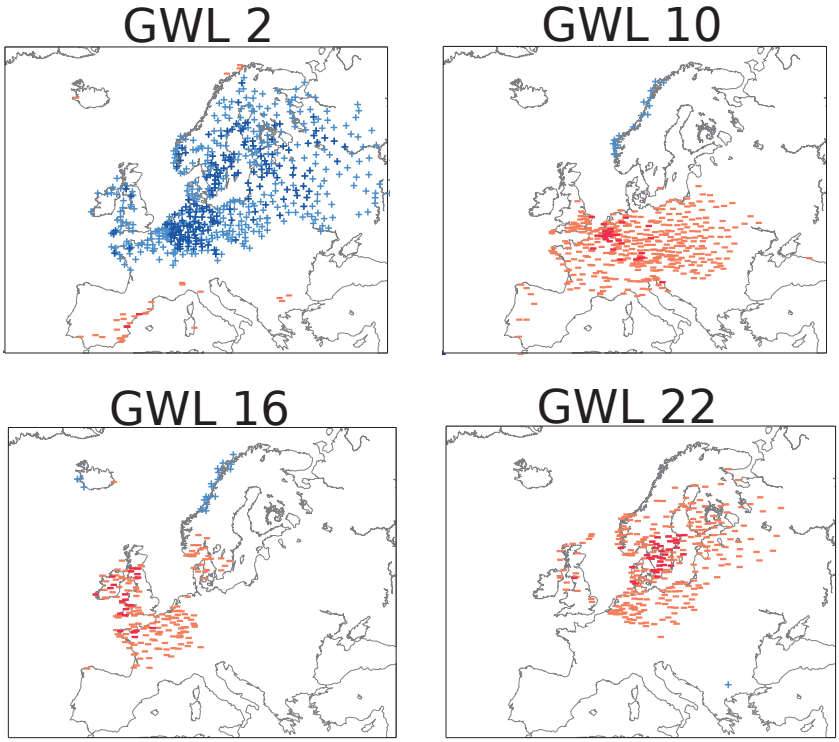

Figure 12: Maps showing the correlation between the monthly cloud cover (surface-based visual observations, obtained from the EECRA data set) and the monthly averaged frequency of four of the 29 GWL weather patterns. The markers represent sites where the correlation is statistically significant at the 95 %-level (student's t-test, $p < 0.05$). Blue $+$ markers represent sites of positive correlation between the cloud cover and GWL frequency and red $-$ markers show sites with a negative correlation. The darker blue and red colours represent correlation coefficients that are stronger than ± 0.3.

Equations 6, 7, and 8 describe how an empirical GWL model, $\hat{y}$(year), is constructed based on a daily observational time series, $y(d)$, and the annual mean frequencies f_i(year) of the 29 GWL weather patterns.

$$\hat{y}(\text{year}) = c_0 + \sum_{i=1}^{29} c_i \cdot f_i(\text{year}) \tag{6}$$

$$c_0 = \frac{1}{N} \sum_{d=d_{\text{start}}}^{d=d_{\text{end}}} y(d) \tag{7}$$

$$c_i = \frac{1}{N_i} \sum_{d=d_{\text{start}}}^{d=d_{\text{end}}} \delta_{i,\text{GWL}(d)} y(d) - c_0 \tag{8}$$

where

$$\delta_{i,GWL(d)} = \begin{cases} 1 & if\ \text{GWL}(d) = i \\ 0 & if\ \text{GWL}(d) \neq i \end{cases}$$

$N =$ total number of daily observations

$N_i = \sum \delta_{i,GWL(d)} =$ total number of days classified as GWL i

The annual model described in Equation 6 is equivalent of a daily model with the same value c_i ascribed to all days d_i that have been identified as GWL i ($i \in [1, 29]$). The coefficients c_i are the anomalies of y associated with the weather patterns GWL i during the calibration period, d_{start}–d_{end}.

In paper II, the standard calibration period is 1990–2013, which allows us to compare the empirical GWL models to independent observational data before 1990. In paper III, the GWL models are constructed on a seasonal basis, for spring (March, April, May) and summer (June, July, August). This has the side effect of reducing the calibration data to one fourth compared to the annual models. To compensate for the smaller calibration sample size, a longer calibration period is used, 1964–1993. In the absence of a long period of independent observational data, resampling techniques (permutation test, jackknife) are applied to evaluate the statistical significance and robustness of the GWL models in paper III.

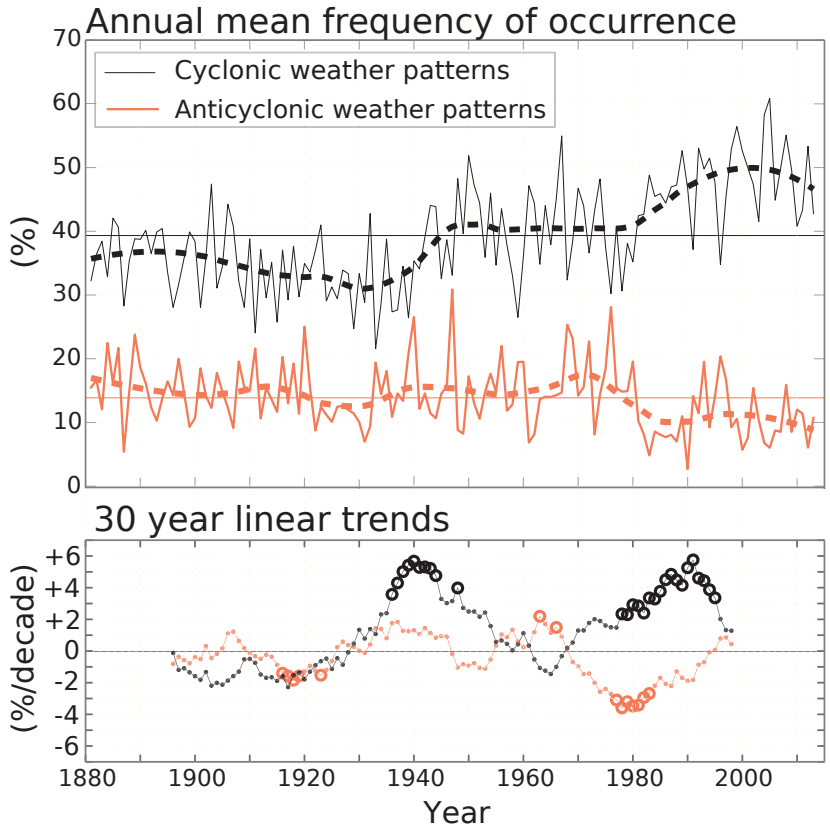

Figure 13: **Trend analysis of the frequency of weather patterns characterised by anti-cyclonic and cyclonic circulation over Fenno-Scandinavia and the Norwegian Sea.** The weather pattern groups are defined in paper III, based on the connection between the observed SW irradiance in northern Europe and the synoptic weather patterns of the Grosswetterlagen (GWL) classification. The cyclonic weather patterns consist of GWL 1, 2, 4, 5, 6, 8, 17 and 29 and the anti-cyclonic weather patterns of GWL 18–24. The cyclonic weather patterns are shown in black and the anti-cyclonic in orange. The upper panel shows the total annual mean frequencies for 1881–2013 (solid lines) and smoothed curves (locally weighted regression smoothing with 40 year window, dashed lines) The lower panel shows the sliding 30 year long linear trends. Here, the x-axis represents the centre year of each period for which a linear trend has been estimated (period = [centre - 15 years, centre + 14 years]). Periods with trends that are significant at the 95 %-level are marked by large circles.

6.2 Changing weather patterns over northern Europe

In paper III, two groups of weather patterns are identified that have a strong influence on the SW irradiance in northern Europe. The first group consists of GWL 18-24, which are characterised by anti-cyclonic weather systems over Scandinavia and the Baltic region. The anti-cyclonic weather patterns are associated with sunnier than usual conditions in northern Europe, with the exception of Iceland. The other group, consists of GWL 1, 2, 4, 5, 6, 8, 17 and 29, which are characterised by cyclonic weather systems over the Norwegian Sea and Scandinavia. The cyclonic weather patterns are associated with reduced SW irradiance in northern Europe, except in Iceland.

The Grosswetterlagen classification represents 15 other synoptic scenarios in addition to the 14 weather patterns discussed above, which account for only about 55 % of all days. Other groupings may be more meaningful to describe the influence of large scale meteorology on SW irradiance in other regions of Europe.

A trend analysis of the frequency of northern European cyclonic and anti-cyclonic weather patterns reveal significant shifts of the atmospheric circulation patterns during the second half of the 20th century (Figure 13). The average frequency of cyclonic weather systems over Scandinavia (GWL 1, 2, 4, 5, 6, 8, 17 and 29) increased from approximately 40 % in the 1960s and 70s to over 50 % after 1990. The occurrence of anti-cyclones over the Scandinavian-Baltic region (GWL 18–24) decreased rapidly during the 1980s from an average of about 15 % before 1970 to around 10 % after 1990. Both the increasing frequency of cyclones and decreasing frequency of anti-cyclones are statistically significant at the 95 %-level, as seen in the lower panel of Figure 13.

7 Summary of papers

This thesis consists of four papers that all concern aspects of atmospheric transfer of SW radiation and the relationship between clouds and SW irradiance.

Papers I–III are about dimming and brightening in northern Europe. The main focus is the influence of clouds and the large scale atmospheric circulation on SW irradiance. The influence of varying aerosol emissions on SW irradiance is assessed directly in paper I by calculating the aerosol optical depth. The impact

of aerosols is assessed indirectly in papers II and III as residual, the portion of SW irradiance that cannot be explained by large scale circulation patterns.

Paper IV is based on work that I did for my master's degree but contains an extended analysis and clearer presentation. It is included here because the paper was written and published during my PhD project. Paper IV deals with the absorption of SW radiation by clouds. It connects to the issue of dimming and brightening because the SW absorptivity of clouds influence the SW signal that satellites retrieve. Hence investigating dimming and brightening via satellite data will depend on the correct estimate of cloud absorption.

Paper I - Decadal variability of clouds, solar radiation and temperature observations at a high-latitude coastal site in Norway

In this work we study the observed variability of shortwave irradiance, clouds and temperature in Bergen. To assess the quality and spatial representativity of the data, we compare observations from independent instruments and neighbouring measurement sites.

Key findings:

- There is a decrease of SW irradiance during the 1970s and 80s in Bergen. The dimming is likely caused by the increasing frequency of clouds, in particular low level clouds, which is observed during this time.
- There is an increase in annual SW irradiance in Bergen after 1990. The brightening appears to be influenced by factors other than cloudiness variations. Calculations of the aerosol optical depth, based on the direct irradiance of hours with an unobscured sun, confirm a decreasing aerosol load after 1990 which may contribute to the recent brightening.
- The strongest dimming and brightening occur in early spring and late summer (March, April and August). The seasonal analysis reveals opposite changes of observed SW irradiance and cloud cover during these months, including the brightening after 1990. This suggests that the early spring/late summer decreasing cloud cover contributes to the annual brightening.

- In winter, the surface air temperature in Bergen is linked to the warming influence of clouds. In all other seasons, the long term warming and multidecadal variability of the North Atlantic sea surface temperature appear to be the more dominant influence on local air temperature compared to local cloud and SW irradiance variations.

Paper II - Influence of synoptic weather patterns on local cloud and solar variability in Bergen, Norway

In this paper, the relationship between the large scale circulation over Europe and the North Atlantic and local surface conditions in Bergen is explicitly addressed. To this end, a method of constructing empirical models of local solar and cloud variables based on the frequency of the Grosswetterlagen (GWL), a European weather pattern classification was developed.

Key findings:

- The empirical linear GWL models successfully reproduce the observed cloud and solar changes during the dimming in the 1970s and 80s in Bergen. This indicates that the cloud and solar changes during this period are due to shifting weather patterns.

- The dimming in the 1970s and 80s is traced to an increasing frequency of cyclonic weather patterns and decrease of the frequency of anticyclonic weather patterns over northern Europe.

- At sites where the large-scale circulation changes have a dominant influence on local cloud variability, as is the case in Bergen, the empirical GWL model can be used to extend observational cloud records by more than 70 years, back to 1881.

- The recent brightening period in Bergen after 1990 is not fully reproduced by the GWL model of normalised SW irradiance. The discrepancy between modelled and observed SW irradiance indicate that factors other than large scale circulation caused the brightening. The decreasing aerosol optical depth discussed in paper I is a likely candidate.

Paper III - Influence of synoptic weather patterns on solar irradiance variability in northern Europe

In this study, the influence of atmospheric circulation on SW irradiance at ten European sites north of 55°N is assessed. Using the method described in paper II, empirical models of normalised SW irradiance are constructed based on the frequency of the individual Grosswetterlagen. The empirical linear GWL models are used to separate the influence of 'natural' SW variability from the direct and indirect effect of varying aerosol emissions. The focus is on spring and summer because of the short day length at high-latitude sites in the winter half-year. This paper explores the spatial footprint of the GWL models in the distribution of SW dimming and brightening.

Key findings:

- The GWL models cannot explain all of the observed SW irradiance variability in northern Europe. At many sites, there is a residual SW irradiance trend. From the 1950s/60s to the 1980s, a weak and in most cases not statistically significant residual dimming is observed. After 1990, a more pronounced and at many sites statistically significant residual brightening was detected.
- The discrepancy between observed and modelled SW irradiance can be interpreted as the influence of factors other than the large scale circulation. The significant residual brightening after 1990 indicates that reduced aerosol emissions in recent decades have had a significant effect on the SW irradiance at many sites in northern Europe.
- In spring, the large scale patterns contribute to the SW irradiance reduction in the 1970s and 80s via a decreasing frequency of anti-cyclonic and increase frequency of cyclonic weather patterns.
- In summer (June, July, August), there is a temporary increase of SW irradiance in the 1970s at many sites which is linked to changes in the frequency of anti-cyclonic and cyclonic weather patterns centred over Scandinavia and the north Atlantic.
- The large-scale circulation changes in summer may be related to a northward shift in the North Atlantic storm track.

Paper IV - SW absorption in the atmosphere: reconciling observations and calculations

The absorption of SW radiation by clouds is a topic surrounded by contradictory reports. Some studies have found no significant difference between observed and model predicted SW absorption while others have reported hugely underestimated SW absorption by radiative transfer models in a cloudy atmosphere. In this study, values of column SW absorption are calculated for a tropical island site, Manus, using collocated satellite and surface-based observations. The surface data are averaged over time (30 minutes to 3 hours) to compensate for the field of view difference between surface and satellite-based instruments. Comparing the observed SW absorption to radiative transfer model (RTM) output indicates that the radiative transfer models appear to underestimate the SW absorption. However, a closer look reveals that observational sampling issues contribute to the apparent discrepancy.

Key findings:

- The SW absorption obtained from collocated surface and satellite observations have an unrealistic range, including negative absorption values. This is most likely because of the a difference in the field of view between surface and and satellite-based instruments. High SW absorption values obtained from collocated satellite and surface based SW measurements are shown to correspond to occasions of large field of view mismatch.

- There are indications that insufficient averaging of surface data contributes to the apparent SW absorption bias. It is concluded that averaging surface data over 3 hours or less is not always sufficient to eliminate sampling issues.

- The possibility that shortcomings of the radiative transfer models contribute to the discrepancy in SW absorption values cannot be excluded. For example, the increased absorption in a 3D scattering cloud field may be a contributing factor to the observation-model bias.

8 Main conclusions and outlook

This thesis investigates the decadal variability of SW irradiance in northern Europe and the factors that contribute to variations of SW attenuation in the atmosphere.

Previous observational studies of SW irradiance in Europe have reported predominantly negative SW irradiance trends from the 1950s to the late 1980s, a dimming, followed by positive trends at many sites in the last two decades, a brightening (Wild, 2012). However, at many sites the estimated SW irradiance trends are not statistically significant, as demonstrated by the trend analysis in Chapter 5.4. Based on statistical tests shown in Figures 6 and 7, it is not clear that there even is a significant dimming and brightening in Europe. These results are in line with previous studies of dimming and brightening at individual sites in central and northern Europe (Norris and Wild, 2007; Chiacchio and Wild, 2010). On the other hand, there are striking regional similarities of the decadal SW irradiance variability in Europe. Even though the observed SW irradiance trends are not significant at many of the individual sites, the common regional tendencies imply that the SW irradiance is influenced by a large scale atmospheric process that varies considerably on decadal time scales. The individual time series may be averaged regionally or for grid boxes to isolate the non-local dimming or brightening (Gilgen et al., 1998, 2009). Varying amounts of atmospheric aerosol, humidity, and clouds, and the interactions among these factors are likely candidates to explain the observed SW irradiance variability in Europe. Differences in dimming and brightening within and between regions of Europe provide some clues to the relative importance of the SW attenuating factors.

Based on the regionally and annually averaged SW irradiance time series in Figure 8, there is a significant dimming in northern Europe from the 1960s to around 1990, but no significant subsequent brightening (question 1 posed in Chapter 2). The seasonal analysis in paper III indicate that there is a significant brightening in northern Europe after 1990 in spring. The cloud analysis in papers I and II show that in Bergen, observations are compatible with a cloud induced SW irradiance change (question 2). This is not the case at all other northern European sites (Stjern et al., 2009). The results of papers I–III suggest that varying aerosol emissions have affected the SW irradiance in northern Europe, most notably during the recent brightening period (question 3). However, the

increasing frequency of cyclonic weather patterns over the Norwegian Sea and northern Europe in the 1980s (Figure 13) has likely contributed to the dimming in the region (question 4).

In papers II and III, the relationship between large scale weather patterns and local SW irradiance is established by constructing empirical statistical models based on the Grosswetterlagen. The GWL models are assumed to represent the portion of SW irradiance variability that is associated with varying large scale weather patterns. At a site like Bergen where the GWL model fits well with the observed SW irradiance variability (see paper II), the interpretation is straight forward: the SW irradiance variations are driven primarily by large-scale atmospheric circulation. However, when the GWL model generated time series does not follow the observed SW irradiance closely, as is the case at several other sites in northern Europe, the results are more difficult to interpret. In paper III, discrepancies between observed and modelled normalised SW irradiance are detected at many sites. Hence, SW variability may be caused by factors other than atmospheric circulation, e. g. indirect and direct aerosol effects. On the other hand, the model may also fail to reproduce the locally observed SW variability due to model construction issues, or because the GWL classification does not identify the large scale weather patterns that govern cloud and humidity distribution at other locations. The German-centric definition of the Grosswetterlagen patterns is a drawback when using it to investigate meteorological shifts in the radiative climate regions outside of central Europe. An alternative approach could be to define weather patterns by objective classification (Schubert, 1994; James, 2006).

Meteorological reanalysis is the process of assimilating observations to provide a consistent and complete record of the current state of the atmosphere. Reanalysis data are used as initial conditions for weather forecasting models but the historic assimilation can also be a useful tool in climate and weather research. Generally, meteorological reanalysis data are produced without information about changing aerosol concentrations. Therefore the SW irradiance of reanalysis data sets can be assumed to be representative of the SW influence of the atmospheric circulation and clouds, similarly to the GWL models. It may be interesting in future studies to compare reanalysis data to GWL model simulated SW irradiance or sunshine duration. The reanalysis SW irradiance data itself can also be used to separate the influence of weather patterns from the aerosol emissions. Comparisons of SW irradiance observations with the ERA-40 reanal-

ysis data (Uppala et al., 2005) have found that the reanalysis does not fully reproduce the observed dimming and brightening in Europe Wild and Schmucki (2010). Compared to the reanalysis data, the GWL models presented in this thesis have added value because they provide a direct link between specific weather patterns and the local surface SW irradiance. The GWL frequencies can thus be used to quantify and describe how changing frequencies of specific weather patterns influence the local radiative climate in different periods, as demonstrated in papers II and III. The synoptic weather patterns takes you one step closer to an understanding of the circulation changes that underlies the weather pattern-driven SW irradiance change.

References

Alados-Arboledas, L., Olmo, F. J., Ohvril, H. O., Teral, H., and Arak, M. (1997). Evolution of solar radiative effects of Mount Pinatubo at ground level. *Tellus B*, 49(B):190–198.

Barker, T. (2007). Climate Change 2007 : An Assessment of the Intergovernmental Panel on Climate Change. *Change*, 446(November):12–17.

Baur, F., Hess, P., and Nagel, H. (1944). Kalender der Großwetterlagen Europas 1881-1939. Technical report, Forschungsinstitut für langfristige Wettervorhersage, Bad Homburg.

Bengtsson, L., Hodges, K. I., and Roeckner, E. (2006). Storm tracks and climate change. *Journal of Climate*, 19:3518–3543.

Blain, G. G. C. (2013). The modified Mann-Kendall test: on the performance of three variance correction approaches. *Bragantia, Campinas*, 72(4):416–425.

Chiacchio, M., Ewen, T., Wild, M., and Arabini, E. (2010). Influence of climate shifts on decadal variations of surface solar radiation in Alaska. *Journal of Geophysical Research*, 115:D00D21.

Chiacchio, M. and Vitolo, R. (2012). Effect of cloud cover and atmospheric circulation patterns on the observed surface solar radiation in Europe. *Journal of Geophysical Research*, 117(D18):D18207.

Chiacchio, M. and Wild, M. (2010). Influence of NAO and clouds on long-term seasonal variations of surface solar radiation in Europe. *Journal of Geophysical Research*, 115:D00D22.

Cutchis, P. (1974). Stratospheric ozone depletion and solar ultraviolet radiation on Earth. *Science (New York, N.Y.)*, 184(4132):13–9.

Durack, P. J., Wijffels, S. E., and Matear, R. J. (2012). Ocean salinities reveal strong global water cycle intensification during 1950 to 2000. *Science (New York, N.Y.)*, 336(6080):455–8.

EEA Technical report (2014). European Union emission inventory report 1990-2012 under the UNECE Convention on Long-range Transboundary Air Pollution (LRTAP). Technical Report 12, European Environment Agency, Luxembourg.

Ellis, J. S. and Vonder Haar, T. H. (1977). Application of meteorological satellite visible channel radiances for determining solar radiation reaching the ground. In *Conference on Aerospace and Aeronautical Meteorology and Symposium on Remote Sensing from Satellites; 7th; November 16-19, 1976; Melbourne, FL*, pages 242–244.

Ermolli, I., Matthes, K., Dudok de Wit, T., Krivova, N. a., Tourpali, K., Weber, M., Unruh, Y. C., Gray, L., Langematz, U., Pilewskie, P., Rozanov, E., Schmutz, W., Shapiro, a., Solanki, S. K., and Woods, T. N. (2013). Recent variability of the solar spectral irradiance and its impact on climate modelling. *Atmospheric Chemistry and Physics*, 13(8):3945–3977.

Fröhlich, C. (2009). Evidence of a long-term trend in total solar irradiance. *Astronomy and Astrophysics*, 501(3):L27–L30.

Fröhlich, C. (2011). Total Solar Irradiance: What Have We Learned from the Last Three Cycles and the Recent Minimum? *Space Science Reviews*, 176(1-4):237–252.

Gilgen, H. and Ohmura, A. (1999). The global energy balance archive. *Bulletin of the American Meteorological Society*, 80(5):831–850.

Gilgen, H., Roesch, A., Wild, M., and Ohmura, A. (2009). Decadal changes in shortwave irradiance at the surface in the period from 1960 to 2000 estimated from Global Energy Balance Archive Data. *Journal of Geophysical Research*, 114:D00D08.

Gilgen, H., Wild, M., and Ohmura, A. (1998). Means and Trends of Shortwave Irradiance at the Surface Estimated from Global Energy Balance Archive Data. *Journal of Climate*, 11(8):2042–2061.

Goswami, D. Y., Kreith, F., and Kreider, J. F. (2000). *Principles of Solar Engineering*. Taylor & Francis, Philadelphia, PA, USA, 2nd edition.

Goudie, A. S. (2009). Dust storms: recent developments. *Journal of environmental management*, 90(1):89–94.

Hahn, C. J. and Warren, S. G. (1999). Extened Edited Synoptic Cloud Reports From Ships and Land Stations Over the Globe, 1952-1996. Technical report, Environmental Sciences Division, United States Department of Energy, Oak ridge, TN.

Haigh, J. D., Winning, A. R., Toumi, R., and Harder, J. W. (2010). An influence of solar spectral variations on radiative forcing of climate. *Nature*, 467(7316):696–9.

Hamed, K. H. (2009). Exact distribution of the MannâĂŞKendall trend test statistic for persistent data. *Journal of Hydrology*, 365(1-2):86–94.

Hamed, K. H. and Ramachandra Rao, A. (1998). A modified Mann-Kendall trend test for autocorrelated data. *Journal of Hydrology*, 204(1-4):182–196.

Hanson, K. J. (1971). Studies of cloud and satellite parametrizations of solar irradiance at the earth's surface. In *Proceedings of Miami workshop on remote sensing*, pages 133–148, Washington DC. U.S. Department of Commerce.

Hathaway, D. H. (2010). The solar cycle. *Living Reviews in Solar Physics*, 7(1):http://www.livingreviews.org/lrsp–2010–1 cited Sep.

Haywood, J. M., Bellouin, N., Jones, A., Boucher, O., Wild, M., and Shine, K. P. (2011). The roles of aerosol, water vapor and cloud in future global dimming/brightening. *Journal of Geophysical Research*, 116(D20):D20203.

Hinkelman, L. M., Stackhouse, P. W., Wielicki, B. A., Zhang, T., and Wilson, S. R. (2009). Surface insolation trends from satellite and ground measurements: Comparisons and challenges. *Journal of Geophysical Research*, 114:D00D20.

Holton, J. R. (2004). *An introduction to dynamic meteorology*. Elsevier Academic Press, Burlington, MA 01803, USA, 4 edition.

Hudson, J. (1993). Cloud condensation nuclei. *Journal of Applied Meteorology*, 32:596–607.

Iqbal, M. (1983). *An introduction to solar radiation*. Academic press Canada, Ontario, 1 edition.

James, P. M. (2006). An objective classification method for Hess and Brezowsky Grosswetterlagen over Europe. *Theoretical and Applied Climatology*, 88(1-2):17–42.

Kanamitsu, M., Ebisuzaki, W., Woollen, J., Yang, S.-K., Hnilo, J. J., Fiorino, M., and Potter, G. L. (2002). NCEP-DOE AMIP-II Reanalysis (R-2). *Bulletin of the American Meteorological Society*, pages 1631–1643.

Katz, J. L. and Ostermier, B. J. (1967). Diffusion CloudâĂŘChamber Investigation of Homogeneous Nucleation. *The Journal of Chemical Physics*, 47(2):478–487.

Kendall, M. G. (1970). *Rank Correlation Methods*. Hafner, New York, 2nd edition.

Kokhanovsky, A. (2004). Optical properties of terrestrial clouds. *Earth-Science Reviews*, 64:189–241.

Kopp, G. and Lean, J. L. (2011). A new, lower value of total solar irradiance: Evidence and climate significance. *Geophysical Research Letters*, 38(1):n/a–n/a.

Koren, I. and Feingold, G. (2011). Aerosol-cloud-precipitation system as a predator-prey problem. *Proceedings of the National Academy of Sciences of the United States of America*, 108(30):12227–32.

Lean, J. L. (2010). Cycles and trends in solar irradiance and climate. *WIREs Climate Changes*, 1(January/February):111–122.

Liepert, B. G. (2002). Observed reductions of surface solar radiation at sites in the United States and worldwide from 1961 to 1990. *Geophysical Research Letters*, 29(10):1421.

Liepert, B. G. and Romanou, A. (2005). Global dimming and brightening and the water cycle. *Bulletin of the American Meteorological Society*, pages 622–623.

Liley, J. B. (2009). New Zealand dimming and brightening. *Journal of Geophysical Research*, 114:D00D10.

Magnus, J. R., Melenberg, B., and Muris, C. (2011). Global Warming and Local Dimming: The Statistical Evidence. *Journal of the American Statistical Association*, 106(494):452–464.

McCabe, G. J. (2002). A step increase in streamflow in the conterminous United States. *Geophysical Research Letters*, 29(24):2185.

Miller, J. D., Skinner, C. N., Safford, H. D., Knapp, E. E., and Ramirez, C. M. (2012). Trends and causes of severity, size, and number of fires in northwestern California, USA. *Ecological applications : a publication of the Ecological Society of America*, 22(1):184–203.

Murphy, D. M., Solomon, S., Portmann, R. W., Rosenlof, K. H., Forster, P. M., and Wong, T. (2009). An observationally based energy balance for the Earth since 1950. *Journal of Geophysical Research*, 114(D17):D17107.

Norris, J. R. and Wild, M. (2007). Trends in aerosol radiative effects over Europe inferred from observed cloud cover, solar âĂIJdimming,âĂİ and solar âĂIJbrighteningâĂİ. *Journal of Geophysical Research*, 112(D8):D08214.

Ohmura, A. (2009). Observed decadal variations in surface solar radiation and their causes. *Journal of Geophysical Research*, 114:D00D05.

Ohmura, A., Dutton, E. G., Forgan, B., Fröhlich, C., Gilgen, H., Hegner, H., Heimo, A., König-Langlo, G., McArthur, B., Müller, G., Philipona, R., Pinker, R., Whitlock, C. H., Dehne, K., and Wild, M. (1998). Baseline Surface Radiation Network (BSRN/WCRP): New Precision Radiometry for Climate Research. *Bulletin of the American Meteorological Society*, 79(10):2115–2136.

Pierce, D. W., Gleckler, P. J., Barnett, T. P., Santer, B. D., and Durack, P. J. (2012). The fingerprint of human-induced changes in the ocean's salinity and temperature fields. *Geophysical Research Letters*, 39(21):n/a–n/a.

Pinker, R., Frouin, R., and Li, Z. (1995). A review of satellite methods to derive shortwave irradiance. *Remote Sensing of Environment*, 51:108–124.

Reda, I., Stoffel, T., and Myers, D. (2003). A method to calibrate a solar pyranometer for measuring reference diffuse irradiance. *Solar Energy*, 74(2):103–112.

Sanchez-Lorenzo, A., Calbó, J., Brunetti, M., and Deser, C. (2009). Dimming/brightening over the Iberian Peninsula: Trends in sunshine duration and cloud cover and their relations with atmospheric circulation. *Journal of Geophysical Research*, 114:D00D09.

Sanchez-Lorenzo, A., Calbó, J., and Martin-Vide, J. (2008). Spatial and Temporal Trends in Sunshine Duration over Western Europe (1938-2004). *Journal of Climate*, 21(22):6089–6098.

Schmocker-Fackel, P. and Naef, F. (2010). More frequent flooding? Changes in flood frequency in Switzerland since 1850. *Journal of Hydrology*, 381(1-2):1–8.

Schubert, S. (1994). A weather generator based on the European 'Grosswetterlagen'. *Climate Research*, 4:191–202.

Smith, S. J., Conception, E., Andres, R., and Lurz, J. (2004). Historical sulfur dioxide emissions 1850-2000: Methods and results. Technical Report January, Pacific Northwest National Laboratory, U.S. Department of Energy, College Park, Maryland.

Stanhill, G. (2003). Through a glass brightly : Some new light on the Campbell Stokes sunshine recorder. *Weather*, 58(January).

Stanhill, G. and Cohen, S. (2001). Global dimming: a review of the evidence for a widespread and significant reduction in global radiation with discussion of its probable causes and possible agricultural consequences. *Agricultural and Forest Meteorology*, 107(4):255–278.

Stine, A. R. and Huybers, P. (2014). Arctic tree rings as recorders of variations in light availability. *Nature communications*, 5(May):3836.

Stjern, C. W., Kristjánsson, J. E., and Hansen, A. W. (2009). Global dimming and global brightening - An analysis of surface radiation and cloud cover data in northern Europe. *International Journal of Climatology*, 29:643–653.

Stokes, G. M. and Schwartz, S. E. (1994). The Atmospheric Radiation Measurement (ARM) Program: Programmatic Background and Design of the Cloud and Radiation Test Bed. *Bulletin of the American Meteorological Society*, 75(7).

Streets, D. G., Yan, F., Chin, M., Diehl, T., Mahowald, N., Schultz, M., Wild, M., Wu, Y., and Yu, C. (2009). Anthropogenic and natural contributions to regional trends in aerosol optical depth, 1980âĂŞ2006. *Journal of Geophysical Research*, 114:D00D18.

Tang, I. N. (1996). Chemical and size effects of hygropscopic aerosols on light scattering coefficients. *Journal of Geophysical Research*, 101(D14):19245–19250.

Uppala, S. M., Källberg, P. W., Simmons, A. J., Andrae, U., Bechtold, V. D. C., Fiorino, M., Gibson, J. K., Haseler, J., Hernandez, A., Kelly, G. A., Li, X., Onogi, K., Saarinen, S., Sokka, N., Allan, R. P., Andersson, E., Arpe, K., Balmaseda, M. A., Beljaars, A. C. M., Berg, L. V. D., Bidlot, J., Bormann, N.,

Caires, S., Chevallier, F., Dethof, A., Dragosavac, M., Fisher, M., Fuentes, M., Hagemann, S., Hólm, E., Hoskins, B. J., Isaksen, L., Janssen, P. A. E. M., Jenne, R., Mcnally, A. P., Mahfouf, J.-F., Morcrette, J.-J., Rayner, N. A., Saunders, R. W., Simon, P., Sterl, A., Trenberth, K. E., Untch, A., Vasiljevic, D., Viterbo, P., and Woollen, J. (2005). The ERA-40 re-analysis. *Quarterly Journal of the Royal Meteorological Society*, 131(612):2961–3012.

Wallace, J. M. and Hobbs, P. V. (2006). *Atmospheric Science: An Introductory Survey*. Elsevier Academic Press, 2nd edition.

Wang, K. (2014). Measurement Biases Explain Discrepancies between the Observed and Simulated Decadal Variability of Surface Incident Solar Radiation. *Scientific reports*, 4(1):6144.

Werner, P. C. and Gerstengarbe, F.-W. (2010). Katalog der Großwetterlagen Europas (1881-2009) nach Paul Hess und Helmut Brezowsky, 7. verbesserte und ergänzte Auflage. *PIK report*, 119.

Wild, M. (2009). Global dimming and brightening: A review. *Journal of Geophysical Research*, 114:D00D16.

Wild, M. (2012). Enlightening Global Dimming and Brightening. *Bulletin of the American Meteorological Society*, 93(1):27–37.

Wild, M. and Schmucki, E. (2010). Assessment of global dimming and brightening in IPCC-AR4/CMIP3 models and ERA40. *Climate Dynamics*, 37(7-8):1671–1688.

Wild, M., Trüssel, B., Ohmura, A., Long, C. N., König-Langlo, G., Dutton, E. G., and Tsvetkov, A. (2009). Global dimming and brightening: An update beyond 2000. *Journal of Geophysical Research*, 114(December 1999):D00D13.

Wild, M. F. (1997). *The heat balance of the Earth in General Circulation Model simulations of present and future climates presented by*. PhD thesis, Swiss Federal Institute of Technology Zurich.

Willson, R. C. and Mordvinov, A. V. (2003). Secular total solar irradiance trend during solar cycles 21âĂŞ23. *Geophysical Research Letters*, 30(5):1199.

World Meteorological Organization (2008). Observations of Clouds. In *WMO Guide to Meteorological Instruments and Methods of Observations. Part I. Measurements of Meteorological Variables*, chapter 15.

Wu, Y., Ting, M., Seager, R., Huang, H. P., and Cane, M. A. (2010). Changes in storm tracks and energy transports in a warmer climate simulated by the GFDL CM2 .1 model. *Climate dynamics*, 37(1-2):53–72.

Yang, K., Ding, B., Qin, J., Tang, W., Lu, N., and Lin, C. (2012). Can aerosol loading explain the solar dimming over the Tibetan Plateau? *Geophysical Research Letters*, 39:L20710.

Yue, S. and Pilon, P. (2004). A comparison of the power of the t test, Mann-Kendall and bootstrap tests for trend detection. *Hydrological Sciences - Journal des Sciences Hydrologiques*, 49(1):21–38.